INTERNAL WAVE SHEAR AND DISSIPATION

M. C. Gregg, D. P. Winkel, and T. B. Sanford

Applied Physics Laboratory and School of Oceanography, College of Ocean and Fishery Sciences, University of Washington, Seattle, Washington, 98105-6698

ABSTRACT

With the Multi-Scale Profiler (MSP), we are able to obtain shear spectra extending from vertical scales of hundreds of meters to the viscous cutoff of small-scale turbulence. Comparing shear spectra from five sites reveals varied spectral shapes and amplitudes over 0.01–0.1 cpm (cycles per meter). The amplitudes converge, however, near 0.14 cpm, just beyond the start of the rolloff of the internal wave range of the spectrum. Cross-spectra of the u (east) and v (north) velocity components reveal significant coherence squared, phases of $\approx \pm 90°$, and corresponding asymmetries in clockwise and anticlockwise rotary spectra at the beginning of the rolloff in most spectra. We interpret these signatures of near-inertial motions as evidence that the rolloff is caused by critical layer interactions of waves having vertical scales of about 10 m being advected by larger-scale waves. Similar signatures occur irregularly throughout the rolloff range, usually 0.1–1 cpm, consistent with critical-layer interactions continuing with increasing wavenumber until the waves break down into turbulence. For waves close to the Garrett and Munk spectrum (GM76), this breakdown occurs at wavenumbers larger than 1 cpm. Owing to the variety of spectral shapes at low wavenumbers, variances of kinetic energy and shear do not change in the same proportion when spectra depart from GM76. Spectra from low latitudes in the central Pacific fail to exhibit the inverse dependence on the Coriolis parameter, f, predicted by Munk (1981). Their shape also differs substantially from GM76. Some have lower kinetic energies than mid-latitude spectra but retain comparable shear variances. In addition, all of the low-latitude spectra roll off much more steeply than do the mid-latitude spectra. The steep rolloff forms a weak spectral gap separating internal waves and turbulence.

INTRODUCTION

For several decades, most turbulence in the ocean's interior has been attributed to breaking internal waves, even though the mechanisms of breaking remain obscure. Possibilities include shear instability, advective overturning, strain, and critical layers formed by large waves advecting smaller waves. The probability of breaking is estimated using the Garrett and Munk (1975) model spectrum, $\Phi(\vec{k}, \omega)$, of the wavenumber and frequency content of the internal wave field. Aside from under the arctic ice cap (Levine et al., 1985), observations find internal wave intensities at or above GM, but rarely below, e.g., Smart (1988). Consequently, GM appears to describe the background state, with average forcing in equilibrium with average dissipation by breaking.

We are attempting to observe both equilibrium and nonequilibrium internal wave states and to determine how vertical wavenumber spectra depart from GM, what clues these departures offer about internal wave dynamics, and how they alter $\langle\varepsilon\rangle$, the average turbulent dissipation rate. Here we examine vertical shear spectra obtained with the Multi-Scale Profiler (MSP). The spectra extend from 0.01 cpm (cycles per meter) to the viscous cutoff, usually near 10 cpm. They were obtained at five sites, four of which were used by Gregg (1989) in comparing moments of 10-m-shear with $\langle\varepsilon\rangle$.

In examining the shear spectra, we ask

- How do spectral shapes at low wavenumbers vary with changes in spectral amplitude? Are the variations systematic, and do kinetic energy and shear variances change proportionately?
- Do the spectra change systematically with latitude?
- How do spectra from the thermohaline staircase observed during CSALT compare with spectra at a similar latitude in a normal profile?
- Do the spectra contain signatures of critical layer interactions, proposed by Holloway (1980) as the mechanism causing the rolloff?
- Does the wavenumber at which internal waves roll off vary with spectral amplitude?
- Is Nasmyth's universal spectrum for turbulence in stratified fluids an adequate description of the dissipation range?

BACKGROUND

Spectra of vertical strain (Gregg et al., 1973; Gregg, 1977a) and of vertical shear (Gargett et al., 1981; Sherman and Pinkel, 1991) change from being nearly flat, k_3^0, at low wavenumbers to approximately k_3^{-1} at wavenumbers higher than about 0.1 cpm. We define k_{k-1} as the wavenumber where the rolloff occurs. Munk (1981) incorporates the rolloff into the GM model, but also inadvertently changes the relationship between kinetic energy and shear variance. Consequently, we use the intermediate model, known as GM76, with a modification for the rolloff, as given by Gregg and Kunze (1991).

Holloway (1980) points out that internal waves with short vertical wavelengths are strongly advected by larger, and hence faster, internal waves. Away from inertial and buoyancy frequencies, i.e., $f \ll \omega \ll N$, the horizontal phase speed of internal waves is

$$c_h \approx \frac{N}{\beta} \quad [\text{m s}^{-1}] \tag{1}$$

where β is the vertical wavenumber in radians per meter. For $\beta = 0.063$ m^{-1} ($k_3 = 0.01$ cpm), $c_h \approx 0.09$ m s^{-1}, compared with an rms velocity for the entire wave field of $u_{\text{rms}} = 0.07$ m s^{-1}, obtained by integrating GM76 for $N = 0.0056$ s^{-1} (3 cycles per

hour). With increasing wavenumber, $c_h \rightarrow u_{\rm rms}$, equaling it at $\beta = 0.08$ m^{-1} ($k_3 =$ 0.013 cpm). Holloway convincingly argues that wave/wave interactions cannot be weak for $c_h \leq u_{\rm rms}$. Why then does the shear spectrum remain flat to 0.1 cpm instead of rolling off at $k_3 = 0.01$–0.02 cpm?

In discussing the rolloff, Munk (1981) cites Ericksen (1978), who computes the gradient Richardson number, $Ri \equiv N^2/(\Delta U/\Delta z)^2$, from moored sensors having $\Delta z = 7$ m. A scatter plot shows few values smaller than 1/4, the necessary condition for shear instability. Defining the Richardson function

$$Ri(k_3) \equiv \frac{\langle N^2 \rangle}{\int_0^{k_3} \Phi_{\rm SHEAR}(\xi)\, d\xi} \tag{2}$$

Munk concludes that the internal wave field is characterized by $Ri(k_{k-1}) = \mathrm{O}(1)$ and argues that the rolloff should shift with changes in energy as

$$E \times k_{k-1} = \text{constant} \tag{3}$$

where E is the dimensionless energy density in GM76. This criterion should apply for shear instability, advective overturning, and instability due to lateral strain. Sherman and Pinkel (1991) point out that when $E = E_{\rm GM76}$, $Ri(0.1) \approx 0.5$ and $Ri(k_3) = 1$ occurs well into the rolloff.

Gregg (1977b) interprets the rolloff region of scalar spectra as composed of decaying internal waves and irreversible density finestructure, i.e., density structure produced by mixing. Gargett et al. (1981) interpret the rolloff as the buoyancy subrange of turbulence and take its upper bound as the buoyancy wavenumber

$$k_{\rm B} \equiv \left(\frac{\langle N^2 \rangle^{3/2}}{\langle \varepsilon \rangle} \right)^{1/2} \quad \left[\mathrm{m}^{-1} \right] \tag{4}$$

They identify the corresponding buoyancy length scale, $L_{\rm B} = 2\pi k_{\rm B}^{-1}$, as the vertical scale of the largest overturns. To explore whether the rolloff results from buoyancy-modified turbulence, they assume that the turbulence is controlled only by $\langle N^2 \rangle$ and $\langle \varepsilon \rangle$ and nondimensionalize their spectra using $k_{\rm B}$ and

$$\Phi_{\rm B} \equiv \frac{\langle N^2 \rangle}{k_{\rm B}} \quad \left[\frac{\mathrm{s}^{-2}}{\mathrm{m}^{-1}} \right] \tag{5}$$

In the rolloff region, the scaling reduces amplitude variations among their spectra from a factor of 4 to a factor of 2. The slope of the rolloff is similar to predictions by some theories of the buoyancy subrange (Shur, 1962; Lumley, 1964), but Gargett et al. cannot determine whether the agreement is fortuitous or results from the rolloff actually being a buoyancy subrange.

We believe that the agreement is fortuitous because Gargett et al. are inconsistent in taking $L_{\rm B}$ as the scale of the largest overturns and in identifying the rolloff region with the

buoyancy subrange. Their identification of L_B with the largest overturns has been confirmed by Dillon (1982) and subsequent investigators, who find that root-mean-square (rms) overturning scales are about $1.25(\langle\varepsilon\rangle / \langle N^2\rangle^{3/2})^{1/2}$ or $0.2L_B$ in the notation of Gargett et al. (1981). (Gargett et al. and Dillon differ by 2π in defining the buoyancy scale.) Because the largest overturns must be several times larger than Dillon's rms scale, L_B is a good upper bound. This, however, means that the rolloff region cannot contain three-dimensional turbulence, which is assumed by Shur (1962) and Lumley (1964) when they consider how stratification flattens the overturns to produce anisotropic structures.

In the atmosphere, internal wave shear spectra also roll off as k_3^{-1} at high wavenumbers, but at low wavenumbers the spectra often rise with increasing wavenumber (Smith et al., 1987). This shape so concentrates velocity and shear variance near the rolloff that the waves are sometimes modeled as a single Fourier component. Stratospheric waves originate in the troposphere and grow rapidly with altitude in response to the exponential decrease in air density. As a consequence, the rolloff shifts to lower wavenumbers with increasing altitude, and the shift is attributed to saturation of the wave field. Fritts (1984, 1989) reviews the extensive literature, which includes much debate about the mechanisms saturating the wave field. Dewan and Good (1986) argue that both shear instability and convective overturning produce spectra of the form

$$\Phi_{SAT}(k_3) = \frac{b\langle N^2\rangle}{\beta} \quad \left[\frac{s^{-2}}{m^{-1}}\right] \tag{6}$$

where b is a constant. They obtain $b = 4$ for shear instability when each wavenumber component saturates individually and $b = 1$ for convective instability, leading to the conclusion that waves reach convective instability before shear instability. Dewan and Good also note that turbulent layers can be much thinner than the scale at which the spectrum saturates. The spectrum rolls off because waves at that scale lose energy. However, the turbulent overturns extracting the energy may be only a few percent of the scale of the wave. Smith et al. (1987) conclude that the instability criteria used by Dewan and Good are too large and obtain $b = 1/2$ for a single Fourier component and $b = 1/6$ for a spectrum of superposed waves.

Hines (1991a) holds that the saturated spectrum in the atmosphere results from the same mechanism as proposed by Holloway for the ocean, i.e., by Doppler shifting and critical layer interactions, rather than by shear instability or convective overturning. Furthermore, he develops a spectrum for this mechanism that asymptotically approaches (6) (Hines, 1991b).

Discussions of internal waves in the ocean have concentrated on the extensive observations in the upper ocean at mid-latitude. The limited observations available from the deep ocean (Sanford, 1991) and from low latitudes (Wunsch and Webb, 1979; Eriksen, 1980) appear different. To incorporate the low-latitude observations, Munk (1981) modifies GM76 by replacing the dimensionless energy density, E, with E'/f, where $E' = 8.8 \times 10^{-7}$ and f is the Coriolis parameter. This changes the model from constant energy in the wave field to constant spectral density, thereby accommodating Wunsch and

Webb's report that " ...on the equator the frequency spectrum does not change shape but the vertical and horizontal coherences are much reduced compared to midlatitude values, suggestive of higher modes." With this change, the shear spectrum becomes

$$\Phi_{\mathrm{SHEAR}}(k_3) = \frac{3E'b^3N_0^2}{2j_*\pi f}\frac{\beta^2}{(1+\beta/\beta_*)^2} \quad \left[\frac{\mathrm{s}^{-2}}{\mathrm{m}^{-1}}\right] \tag{7}$$

In their theoretical models of wave/wave interactions, McComas and Müller (1981) and Henyey et al. (1986) give the energy flux through the spectrum as proportional to f. Consequently, $\langle\varepsilon\rangle$ is also proportional to f. Both Müller and Henyey (personal communications, 1990) allow that the f scaling is dictated mostly by the need for correct dimensions rather than by serious consideration of the effect of f on wave/wave interactions. Nevertheless, both predict that for constant shear variance $\langle\varepsilon\rangle \to 0$ approaching the equator. Coupled with Munk's (1981) prediction (7), one would expect to find the anomalous situation of increasing shear variances and decreasing dissipation rates.

OBSERVATIONS AND DATA ANALYSIS

Encompassing a six-fold variation in f, the observations come from one cruise in the Atlantic and two in the Pacific (Table 1). The Atlantic data were taken in October 1985 during CSALT and span the thermohaline staircase lying east of Barbados at pressures of 3–6.5 MPa (Gregg and Sanford, 1987). Retaining much of the steppiness in the density field, the CSALT velocity profiles are not primarily signatures of internal waves but are included for comparison with the other profiles, which are dominated by internal waves in regions with little or no mean shear (Fig. 1). PATCHEX was conducted a year later on the western side of the California Current, and the profiles appear typical of the open ocean, except for ubiquitous salt-stabilized temperature inversions (Gregg and Sanford, 1988). After the primary PATCHEX observations, we worked for two days in a coastal jet off Crescent City, California, obtaining the profiles referred to as PATCHEX north. Both sets of PATCHEX profiles extend to 10 MPa. The following spring, while transiting to and from the equator for TROPIC HEAT 2, we took three test drops to 5 MPa at 6°N and five drops to 10 MPa at 11°N.

Table 1: MSP data sets.

Cruise	Dates	Position	$10^5 f/\mathrm{s}^{-1}$	# Profiles	$p_{\max}$/MPa
CSALT	Nov 23–24, 1985	12°N, 56.5°W	3.02	5	7
PATCHEX	Oct 17–24, 1986	34°N, 127°W	8.13	28	10
PATCHEX north	Oct 26–27, 1986	42°N, 126°W	9.73	5	10
TROPIC HEAT 2	Mar 28–29, 1987	6.0°N, 143.5°W	1.52	3	5
TROPIC HEAT 2	Apr 18–19, 1987	11.5°N, 134.8°W	2.90	5	10

Because GM76 describes the average behavior of random wave fields, we tested the PATCHEX and PATCHEX north shear profiles for randomness by first-differencing u (east) and v (north) with $\Delta z = 10$ m. After WKB scaling, $\Delta u/\Delta z$ and $\Delta v/\Delta z$ have

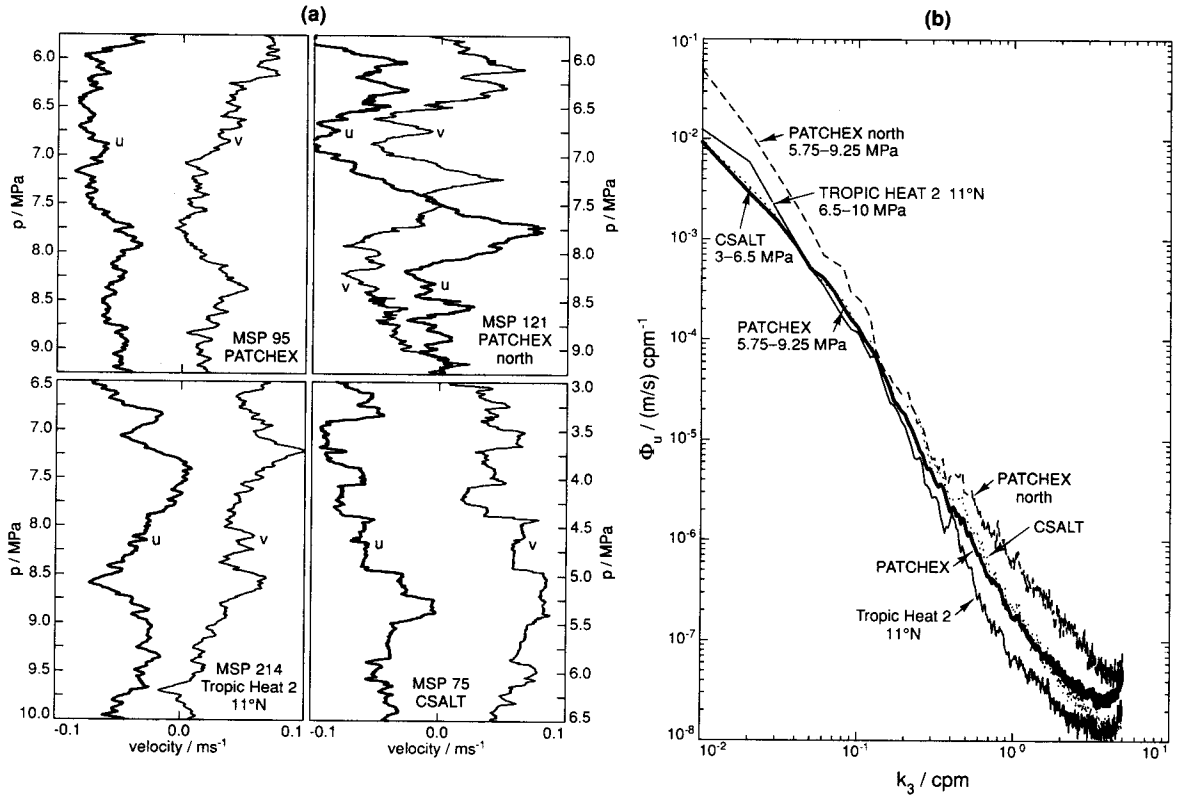

Figure 1: Typical velocity profiles (a) and average velocity spectra (b). PATCHEX north has the largest velocity fluctuations and the highest spectral levels at low and at high wavenumbers. The CSALT profiles show some of the steppiness of the density field, but their average spectrum is similar to that of the PATCHEX profiles. The spectrum for TROPIC HEAT 2 at 11°N is dominated by noise for $k_3 > 3$ cpm. All spectra are slightly aliased just before the Nyquist wavenumber at 5 cpm.

normal probability densities with zero means and are independent of each other (Gregg et al., 1991). In addition, we used the run test (Bendat and Piersol, 1971) and the cumulative periodogram (Jenkins and Watts, 1969) to determine that these shear profiles have no significant departures from vertical randomness. These data sets, therefore, satisfy the criteria for random internal wave fields assumed by Garrett and Munk (1975). The other data sets are too small for adequate testing, but we find no visual suggestions of deterministic features.

To avoid the near-surface internal wave duct, we analyze only data below the shallow thermocline and, when the records are sufficiently long, take two sets of spectra, referred to as shallow and deep. Depending on the record, the sections are 2.5–3.5 MPa thick. Considering all sections, the average buoyancy frequency has a small range, $\langle N^2 \rangle^{1/2} = 0.0028$–$0.0042$ s^{-1}.

The MSP senses velocity with two pairs of electrodes, two airfoil probes, and a two-axis N. Brown acoustic current meter (ACM). The acoustic channels are recorded at 62.5 Hz, corresponding to $\Delta z = 4$ mm at typical fall rates of 0.25 m s^{-1}. To convert the

acoustic data to u and v, we adapt previous models (Evans et al., 1979; Hayes et al., 1984) for the MSP configuration. Corrected velocities are low-passed with a 2-kPa Bartlett filter and digitized at 1 kPa. At low wavenumbers, these data are compared with velocities derived from the motionally induced electromagnetic signals, which are much less sensitive to vehicle motion. At high wavenumbers, we compute velocity from the airfoil probes, which sense fluctuations for 1–2 cpm $< k_3 \leq 100$ cpm.

Data are conditioned for spectral analysis by subtracting the mean, first-differencing, and applying the Hann filter. For the ACM records, u and v are put in real and complex arrays, and Singleton's (1969) algorithm is used to take Fourier transforms of pieces containing 1000 points (corresponding to 1 MPa). This yields two autospectra, $\Phi_{\mathrm{u}}(k_3)$ and $\Phi_{\mathrm{v}}(k_3)$, and the co- and quadspectra, $\Phi^{\mathrm{c}}_{\mathrm{uv}}(k_3)$ and $\Phi^{\mathrm{q}}_{\mathrm{uv}}(k_3)$, all of which are corrected for first-differencing, for the loss in variance to the Hann window, and for the Bartlett window. Successive pieces are overlapped by 50%, resulting in 4–6 pieces for sections of 2.5–3.5 MPa. Wavenumbers are given in cycles per meter as $k_3 = (0.01/\Delta p)$ cpm, where Δp is the pressure interval in megapascals.

For one profile, the degrees of freedom per spectral estimate is

$$\nu_1 = 2L^2/(1.056L - 0.056) \tag{8}$$

where L is the number of pieces overlapped by 50% (D. Percival, personal communication, 1991). After averaging R records, the total number of degrees of freedom is $\nu = R \times \nu_1$. With $L = 6$ and $R = 28$, PATCHEX has $\nu = 321$. At the other extreme, TROPIC HEAT 2 at 6°N has $L = 4$ and $R = 3$, yielding $\nu = 23$. Defining $\hat{\Phi}(k_3)$ as a spectral estimate and $\Phi(k_3)$ as the true spectrum, the 95% confidence limits are

$$\left[\frac{\nu\hat{\Phi}(k_3)}{\chi^2_{\nu;0.025}} \leq \Phi(k_3) \leq \frac{\nu\hat{\Phi}(k_3)}{\chi^2_{\nu;0.975}}\right] \tag{9}$$

where $\chi^2_{\nu;0.025}$ is the chi-square distribution evaluated for ν degrees of freedom and the 0.025 percentile. These limits are plotted as shading around the spectra.

Adding the two autospectra forms the spectrum of total velocity,

$$\Phi_{\mathrm{VEL}}(k_3) = \Phi_u(k_3) + \Phi_v(k_3) \quad [(\mathrm{m/s})^2\ \mathrm{cpm}^{-1}] \tag{10}$$

which is twice the spectrum of specific kinetic energy. Near the Nyquist wavenumber, 5 cpm, all spectra are slightly aliased, in spite of the Bartlett window. Some have negligible noise, e.g., PATCHEX north; others, e.g., TROPIC HEAT 2 at 11°N, become noisy near 3 cpm. Taking the noise level as 1.8×10^{-8} m^2 s^{-1} and the noise bandwidth as 2 cpm gives an rms noise of 0.16 mm s^{-1}.

The velocity spectra are used to compute the shear spectra

$$\Phi_{\mathrm{SHEAR}}(k_3) = (2\pi k_3)^2\ \Phi_{\mathrm{VEL}}(k_3) \quad [\mathrm{s}^{-2}\mathrm{cpm}^{-1}] \tag{11}$$

which are cut off before 2 cpm to avoid noise contamination (Fig. 2).

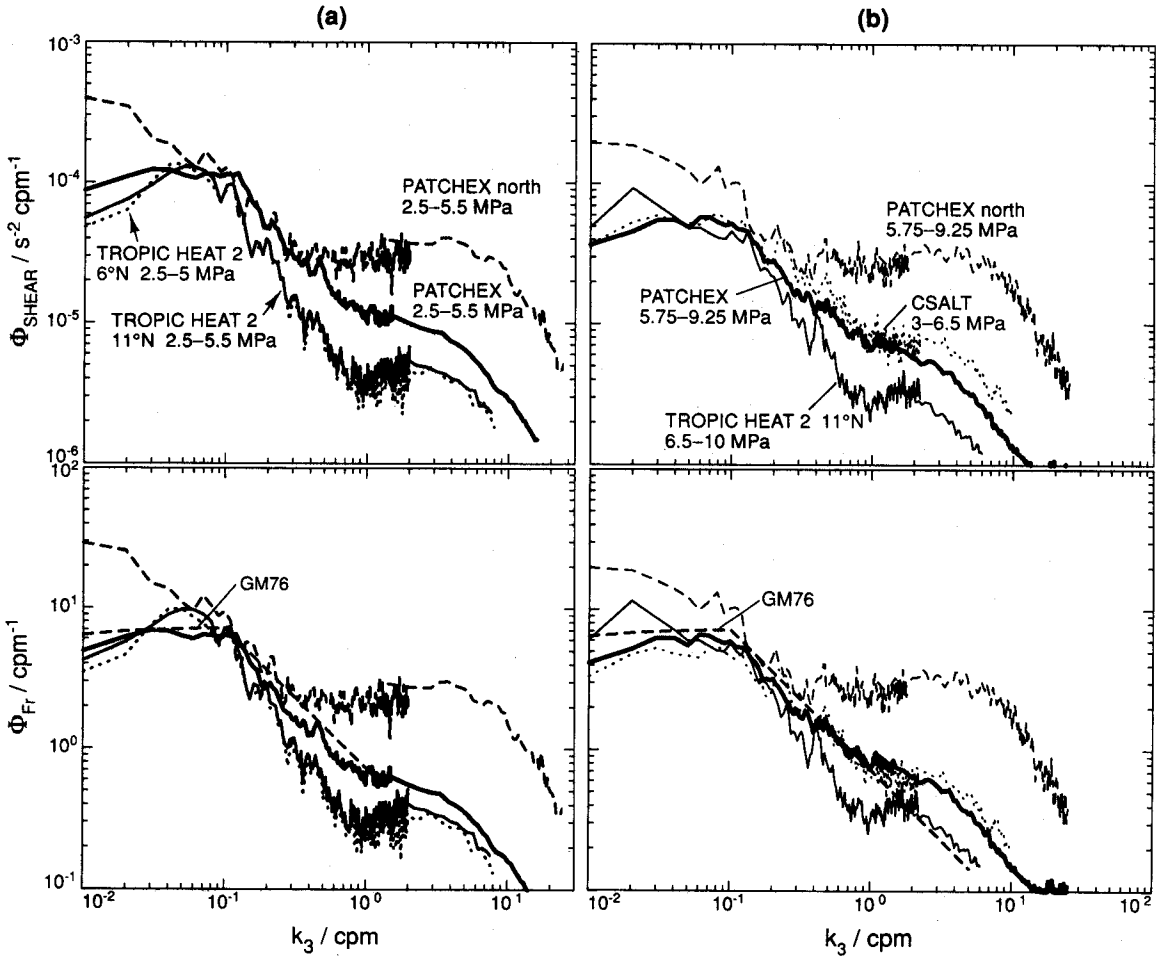

Figure 2: Average shear and Froude spectra for the shallow (a) and deep (b) sections. GM76 is shown on the Froude spectra as a heavy dashed line. Although the Froude spectra differ by a factor of 5 at 0.01 cpm and by 10–20 at high wavenumbers, they have nearly the same amplitude at 0.14 cpm.

To compare shear spectra from records having different stratification, we present them as Froude spectra

$$\Phi_{\mathrm{Fr}}(k_3) \equiv \left\langle N^2 \right\rangle^{-1} \Phi_{\mathrm{SHEAR}}(k_3) \quad [\mathrm{cpm}^{-1}] \tag{12}$$

For reference, we use the Froude spectrum for GM76,

$$\Phi_{\mathrm{Fr}}^{\mathrm{GM76}}(k_3) = \frac{3Eb^3N_0^2}{2j_*\pi} \frac{\beta^2}{(1+\beta/\beta_*)^2} \quad \left[\frac{1}{\mathrm{m}^{-1}}\right] \tag{13}$$

and the saturated atmospheric spectrum with $b = 1/2$,

$$\Phi_{\mathrm{Fr}}^{\mathrm{SAT}}(k_3) = \frac{1}{2\beta} \quad \left[\frac{1}{\mathrm{m}^{-1}}\right] \tag{14}$$

Co-spectra and quadspectra are used for coherence-squared

$$coh^2(k_3) \equiv \frac{\Phi^c_{uv}(k_3)^2 + \Phi^q_{uv}(k_3)^2}{\Phi_u(k_3)\,\Phi_v(k_3)} \tag{15}$$

and phase

$$\phi(k_3) \equiv -\frac{180^\circ}{\pi} \arctan\left(\frac{-\Phi^q_{uv}(k_3)}{\Phi^c_{uv}(k_3)}\right) \tag{16}$$

The sign convention gives $\phi > 0$ when v leads u with increasing pressure. Confidence limits (95%) are computed using Percival (1991).

Because the ACM data are limited to $k_3 \leq 3$–4 cpm, the vertical spectrum is completed using data from the airfoil probes. The two airfoil probes on the MSP are aligned with their sensitive axes in the same direction, which aids in removing spectra contaminated by plankton impacts. Consequently, we analyze the spectrum of one channel, compare with the spectrum of other channel to detect noise spikes, assume horizontal isotropy, and multiply by 2 to obtain $\Phi_{VEL}(k_3)$. For the deep data, spectra are taken over intervals of 0.07–0.08 MPa, again with 50% overlap. For the shallow data, we use a new robust procedure (Hess et al., 1991) and take spectra over 0.02 MPa intervals. Comparisons of the two procedures reveal no significant differences in average spectra. As the airfoils are recorded at 125 Hz, their spectra have many degrees of freedom, e.g., $\nu = 5,253$ for PATCHEX. Consequently, some 95% confidence limits are too narrow to be seen on plots. We form the composite spectra by overlaying spectra from the ACM and airfoil probes, without adjusting amplitudes. Variance-preserving plots show that the dissipation ranges are moderately well resolved, except for the deep spectrum at 11°N, which has the weakest signals (Fig. 3).

At high wavenumbers, the observed spectra are compared with the Nasmyth universal turbulence spectrum (Oakey, 1982). It depends only on the kinematic viscosity and $\langle\varepsilon\rangle$, which we obtain by averaging the ε's we compute routinely over 5 or 10 kPa intervals. Owing to its nonlinear dependence on $\langle\varepsilon\rangle$, the Nasmyth spectrum of $\langle\varepsilon\rangle$ does not equal the average of the individual Nasmyth spectra; numerical simulations show that the two average spectra can diverge significantly, depending on the distribution of ε (H. Seim, personal communication, 1991). Therefore, although the Nasmyth spectrum is a useful approximate reference, we should not expect exact agreement.

AMPLITUDES AND SHAPES

From Figure 2 and from the individual spectra in Figures 4–7, we draw the following conclusions:

- Deep and shallow spectra from the same data set are usually more alike than are spectra from different sets. The shallow spectra from 6°N and 11°N are the exception; they are nearly identical even though they were taken 1000 km and 3 weeks apart.

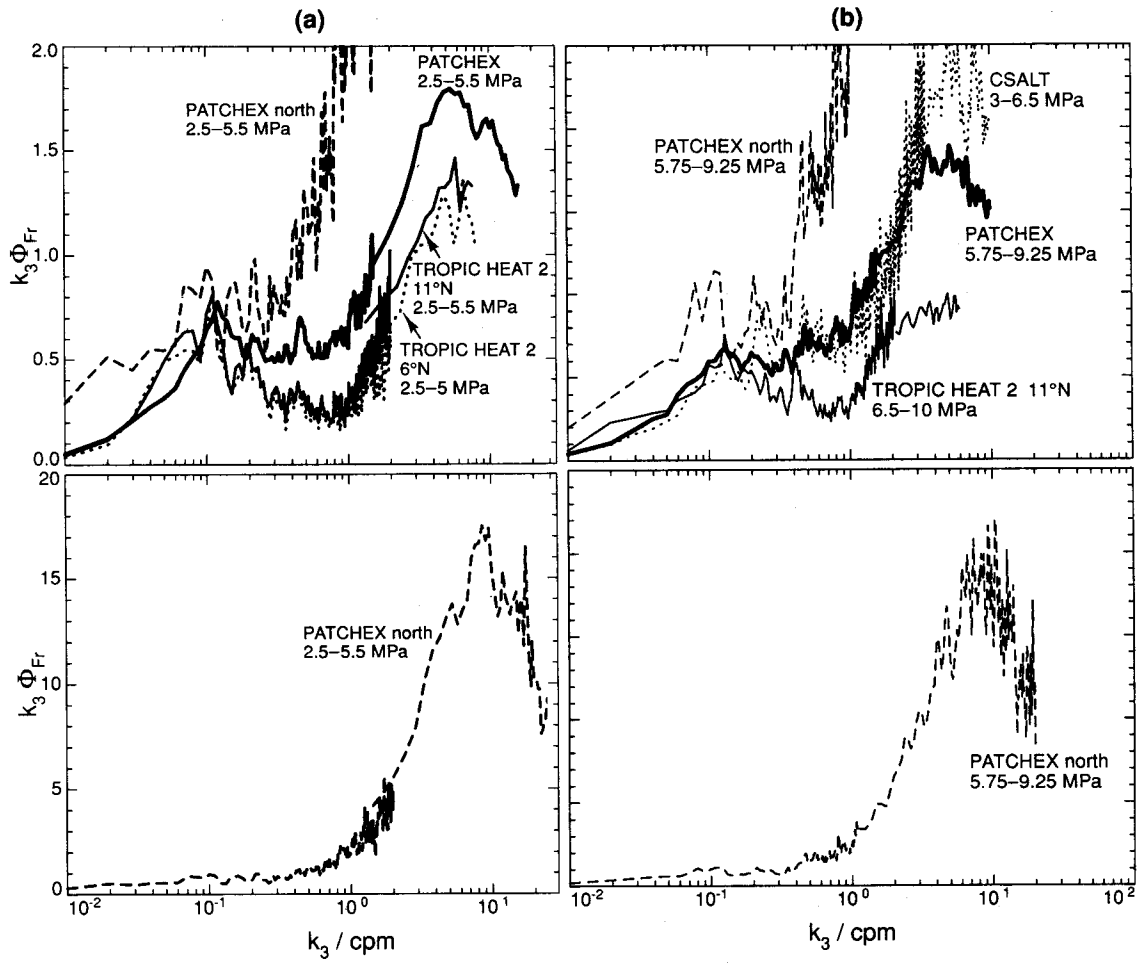

Figure 3: Variance-preserving plots of the spectra in Figure 2.

- All spectra have nearly the same amplitude at 0.14 cpm: (0.65–1.0) × $\Phi_{\mathrm{Fr}}^{\mathrm{GM76}}(1.4)$. By contrast, their amplitudes vary by factors of 5 at 0.01 cpm and 20 in the dissipation range.
- Between 0.01 and 0.1 cpm the spectra exhibit little uniformity in amplitude or shape. Average slopes span -0.55 to +0.75, but in most cases, power laws fail to represent the spectra accurately. Adjustment of the slope to meet GM76 near 0.14 cpm is the only consistent pattern; spectra above GM76 at 0.01 cpm slope downward toward this common point, and those starting below GM76 slope upward.
- The k_3^{-1} rolloff for $k_3 > 0.1$ cpm is the most uniform feature for CSALT, PATCHEX, and PATCHEX north. The rolloff terminates at high wavenumbers where it intersects the Nasmyth spectrum.
- Froude spectra often have local maxima at or near $k_{k^{-1}}$. These are most evident in variance-preserving plots (Fig. 8).

- The three TROPIC HEAT 2 spectra peak near 0.08 cpm and roll off as $k_3^{-1.4}$ for $k_3 > 0.1$ cpm. The steep rolloff produces a weak spectral gap between internal waves and dissipation.
- Turbulence is so weak in most records that the dissipation range follows the Nasmyth spectrum only in the viscous cutoff. PATCHEX north is the exception, with a distinct inertial subrange, extending over half a decade in wavenumbers.

Because most of the spectra change slope near 0.1 cpm, we estimate average slopes using linear fits over 0.01–0.1 cpm and 0.1–1 cpm (Table 2), except where local maxima call for different limits. Most fits over 0.01–0.1 cpm are nominal, as few spectra are truly linear.

Table 2: Average slopes and standard deviations of shear spectra. Owing to particular features, some fits cover restricted intervals: (a) 0.1–0.4 cpm, (b) 0.1–0.37 cpm, (c) 0.01–0.045 cpm, (d) 0.01–0.06 cpm, (e) 0.02–0.1 cpm.

Cruise	p/MPa	0.01–0.1 cpm	0.1–1 cpm
PATCHEX	2.50–5.50	$+0.07 \pm 0.04$	-1.01 ± 0.02
PATCHEX	5.75–9.25	$+0.16 \pm 0.05$	-0.89 ± 0.02
PATCHEX north	2.50–5.50	-0.54 ± 0.04	-0.96 ± 0.08[a]
PATCHEX north	5.75–9.25	-0.33 ± 0.06	-1.03 ± 0.09[b]
TROPIC HEAT 2 6°N	2.50–5.00	$+0.75 \pm 0.13$[c]	-1.43 ± 0.03
TROPIC HEAT 2 11°N	2.50–5.50	$+0.50 \pm 0.04$[d]	-1.38 ± 0.03
TROPIC HEAT 2 11°N	6.50–10.0	-0.55 ± 0.04[e]	-1.37 ± 0.03
CSALT	3.00–6.50	$+0.15 \pm 0.05$	-0.89 ± 0.03

Closest to GM76 throughout the full range of wavenumbers (Fig. 4), the PATCHEX spectra are 0.8 and 0.6 times GM76 at 0.01 cpm. From there, they slope upward as $k_3^{+0.07}$ and $k_3^{+0.16}$. The shallow spectrum makes a sharp transition at the rolloff and initially decreases more steeply than k_3^{-1}, dropping close to the saturated spectrum from the atmosphere which has an amplitude about 50% smaller than GM76 when $b = 1/2$. The deep spectrum rolls off more gradually and stays closer to k_3^{-1}. Near 1 cpm, both PATCHEX spectra cease to roll off as steeply and lie close to the Nasmyth spectrum until 5–8 cpm, where they fail to roll off as steeply as the reference. Such weak turbulence is unlikely to produce an inertial subrange; the viscous rolloff occurs at 2–3 cpm, only an octave past the end of the internal wave part of the spectrum.

The PATCHEX north spectra are 3–4 times GM76 at 0.01 cpm and slope downward to the common point at 0.14 cpm (Fig. 5). By 0.02 cpm, the shallow spectrum is close to an extension of the k_3^{-1} portion of GM76, and it comes closer with increasing wavenumber. The deep spectrum is initially nearly flat and then curves downward to approach the k_3^{-1} extension near 0.08 cpm. For $k_3 > 0.1$ cpm, both PATCHEX north spectra are nearly identical to GM76 until 0.3–0.4 cpm, where they make sharp transitions to the $k_3^{1/3}$ inertial subrange of the turbulent spectrum. (Note that both the ACM and the

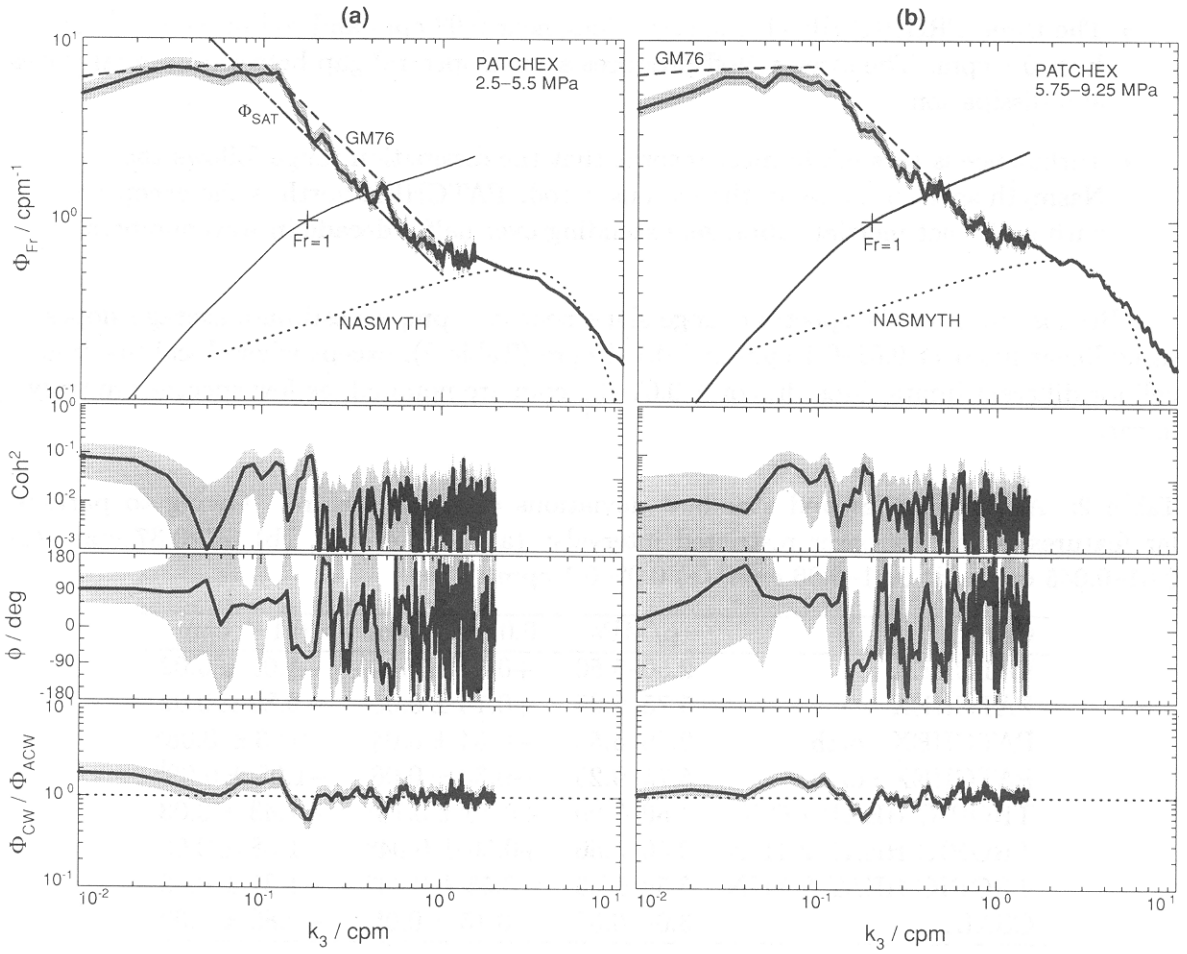

Figure 4: Froude spectra, coherence-squared, phase, and the ratio of clockwise (CW) to anticlockwise (ACW) velocities for PATCHEX. Shading shows 95% confidence limits. Also shown in the top panel are GM76, the saturated internal wave spectrum applied to atmospheric observations ($b = 1/2$), Nasmyth's universal turbulence spectrum in stratified fluids, and the Froude function. Data from the acoustic current meter is used for $k_3 < 1.5$ cpm.

airfoil probes detect the inertial subrange.) Beyond the viscous cutoff, these spectra continue to decrease (Fig. 3), but less steeply than the Nasmyth spectrum. The total range from where the spectrum initially follows $k_3^{+1/3}$ to the peak of the dissipation spectrum is a factor of 6–8, less than a decade. Either the close agreement with the inertial subrange is fortuitous, or it indicates that locally universal turbulence can occur at wavenumbers only 2–3 times larger than the energy-containing overturns.

The shallow spectra for TROPIC HEAT 2 are surprisingly similar, even to their small irregularities (Figs. 2 and 6). From amplitudes 0.6 times GM76 at 0.01 cpm, they slope upward to broad maxima near 0.08 cpm. Their most distinctive feature, however, is the steepness of the rolloff, $k_3^{-1.4}$. The combination of the rise to a peak near 0.08 cpm and the rapid rolloff at high wavenumbers resembles the narrow-band structures observed in

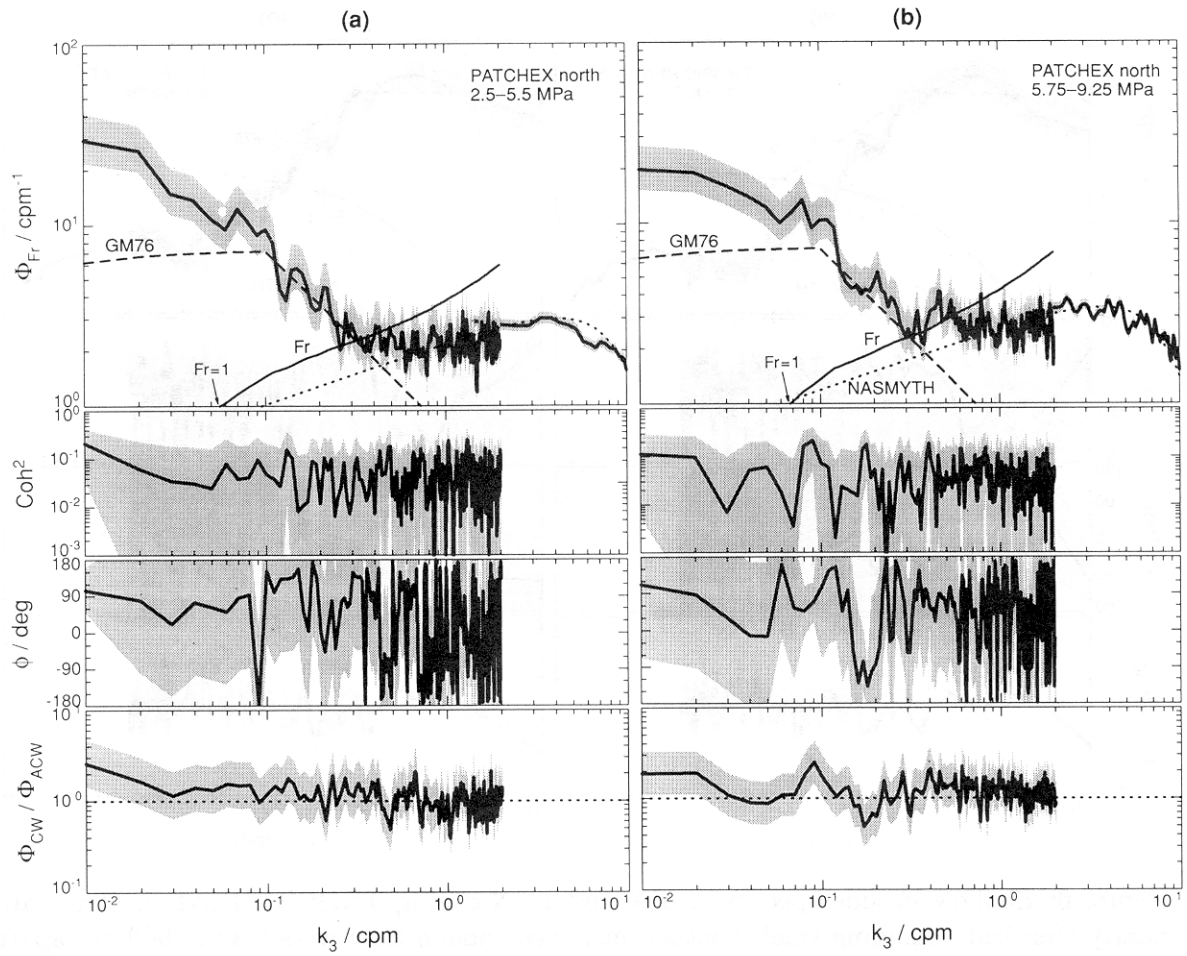

Figure 5: Spectra for PATCHEX north, in the same format as the previous figure.

the stratosphere more than the broad-band fields observed in the mid-latitude ocean. By 1 cpm, the spectra are about 1/3 of GM76. As a result of this steep rolloff, their turbulent spectra are more distinctive than for PATCHEX, even though $\langle \varepsilon \rangle$ is smaller.

The deep spectrum at 11°N starts at GM76, rises to almost twice GM76 at 0.02 cpm, and then slopes gradually downward until just past 0.1 cpm, where it too rolls off rapidly into a weak, but distinct, dissipation range (Fig. 7).

The CSALT spectrum (Fig. 7) is close to the PATCHEX spectra and to GM76, which is unexpected in view of the markedly different appearances of the profiles (Fig. 1). At 0.01 cpm, CSALT is about half of GM76, slightly lower than the PATCHEX spectra. It slopes upward to 0.03 cpm, where it flattens until it rolls off near 0.1 cpm. Unlike PATCHEX, however, this spectrum remains below GM76 when it is nearly flat and consequently rolls off from a lower amplitude than do the other spectra. Initially, the rolloff is less steep than k_3^{-1}, but for $k_3 > 2$ cpm the rolloff does not differ significantly from the model.

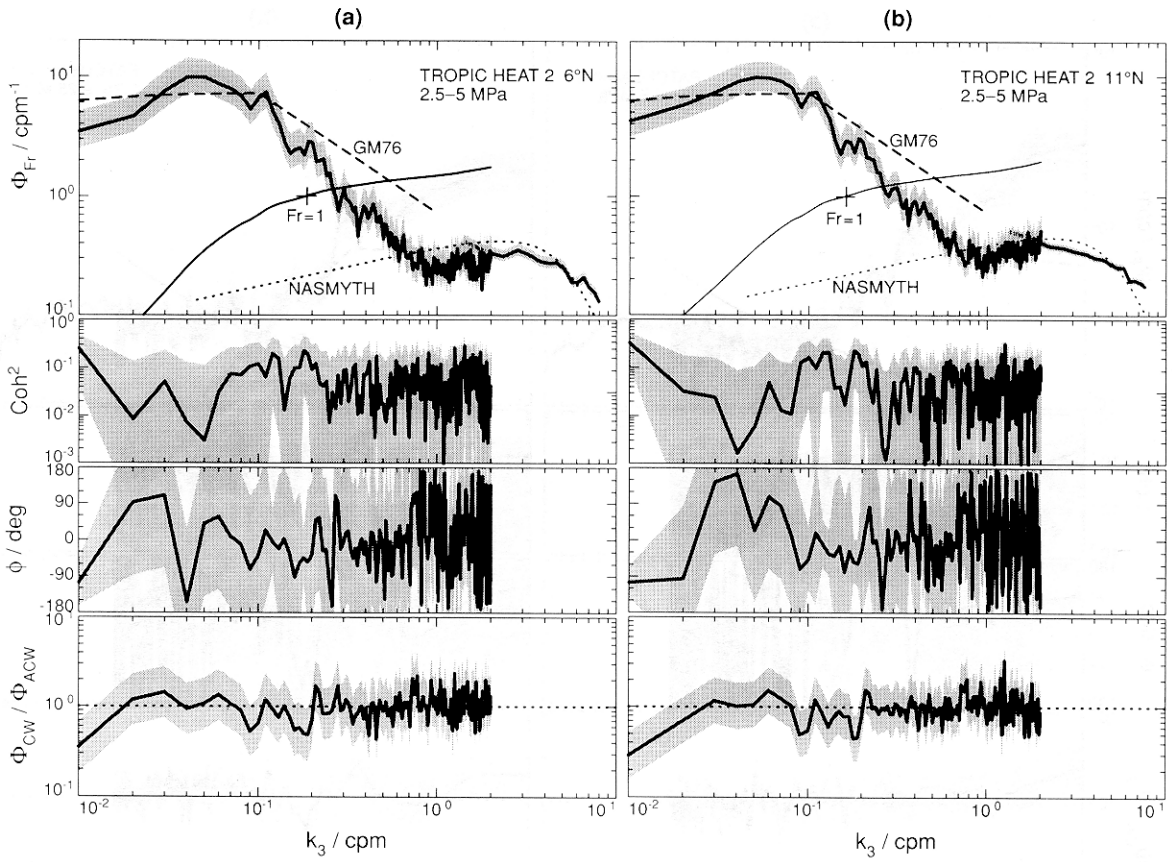

Figure 6: Shallow Froude spectra at 6°N and 11°N during TROPIC HEAT 2. They are nearly identical, including small fluctuations, even though they were taken 1000 km apart at an interval of three weeks.

For this collection of spectra, variance-preserving plots of the internal wave range (Fig. 8) differ considerably, as expected from the differences in the log-log plots. The deep PATCHEX spectrum is closest to GM76 and has the expected concentration of variance in the rolloff (a slope of k_3^{-1} on a log-log plot is flat on a variance-preserving format). The shallow PATCHEX spectrum has a distinct peak at the beginning of the rolloff, and both PATCHEX north spectra have similar peaks at slightly lower wavenumbers, corresponding to the start of their rolloffs. Steep rolloffs of the TROPIC HEAT 2 spectra result in variance contributions decreasing between 0.1 and 1 cpm, constituting the weak spectral gap mentioned previously. Finally, for CSALT the variance is more concentrated at high wavenumbers than for any other spectrum, consistent with concentration of much of the shear across density steps several meters thick (Gregg and Sanford, 1987).

VARIANCES AND SIGNIFICANT WAVENUMBERS

Owing to the variety of their shapes, differences in the spectra cannot be described adequately by E, the dimensionless energy density. In particular, variances of velocity and of shear do not always vary in the same proportion when spectra depart from GM76.

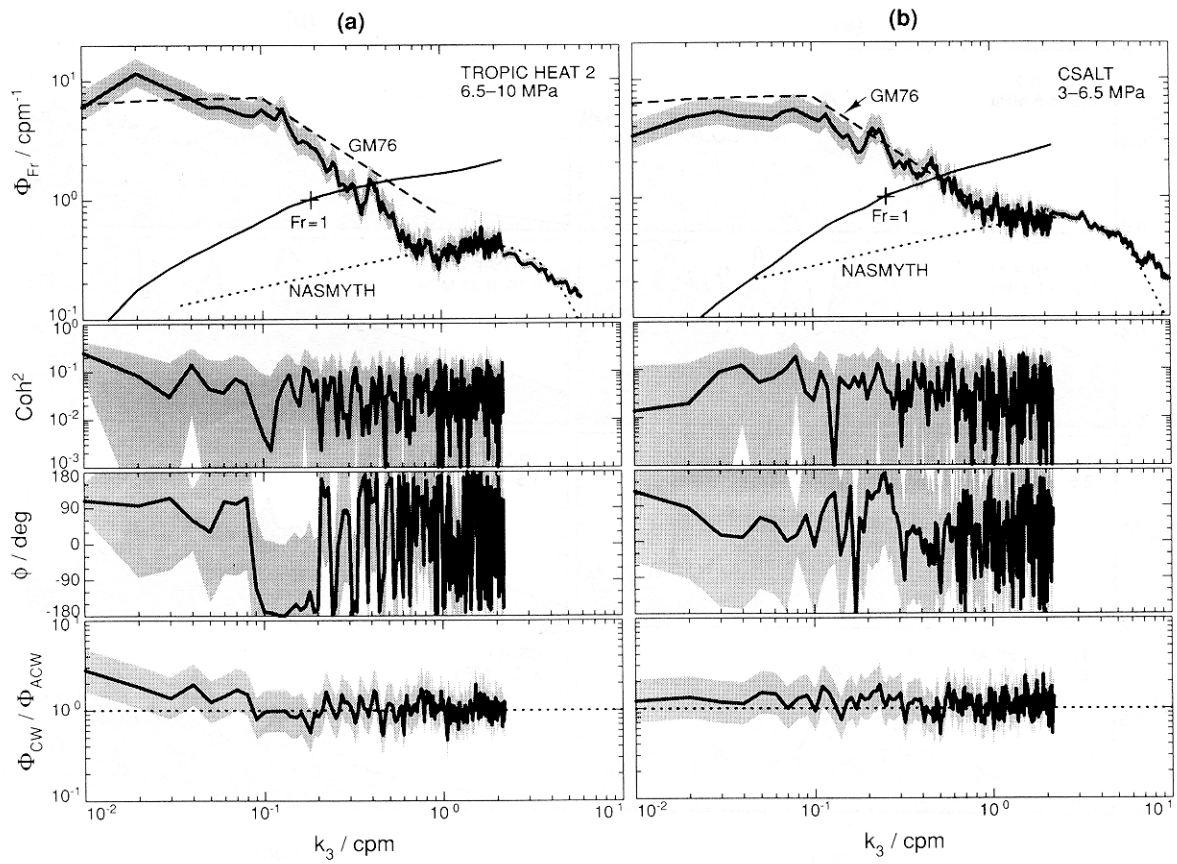

Figure 7: Froude spectra for the deep TROPIC HEAT 2 spectrum and for CSALT.

Because the velocity spectra are 'red,' velocity variances are dominated by the lowest spectral estimate and receive little contribution past the first 4 or 5 estimates. Consequently, they depend on the length of the data window and have relatively few degrees of freedom. As a compromise between length and degrees of freedom, for the longer records we compute $\Phi_{\mathrm{VEL}}(k_3)$ from 2.4 MPa pieces, overlapped by 50%. GM76 is digitized at the same wavenumbers and integrated in the same manner to yield

$$\frac{KE}{KE_{\mathrm{GM}}} \equiv \frac{\int_{0.004}^{k_{\mathrm{IW}}} \Phi_{\mathrm{VEL}}(k_3)\, dk_3}{\int_{0.004}^{k_{\mathrm{IW}}} \Phi_{\mathrm{GM76}}(k_3)\, dk_3} \tag{17}$$

where k_{IW}, the upper limit of the internal wave regime, makes little difference to the integral, and the factors of 1/2 relating kinetic energy and velocity variances cancel. As shown in Table 3, kinetic energy variances are (0.6–4.2)× GM76, consistent with previous observations that internal waves in the open ocean do not fall far below GM76. The contrast between PATCHEX and PATCHEX north appears to be between a typical 'quiet' site in open ocean and an energetic region near strong forcing, presumably the coastal jet several hundred meters above the depths of these spectra.

Contrary to expectations, the low-latitude kinetic energies are less than or only modestly larger than GM76. If the site at 6°N had the same E' as PATCHEX, from

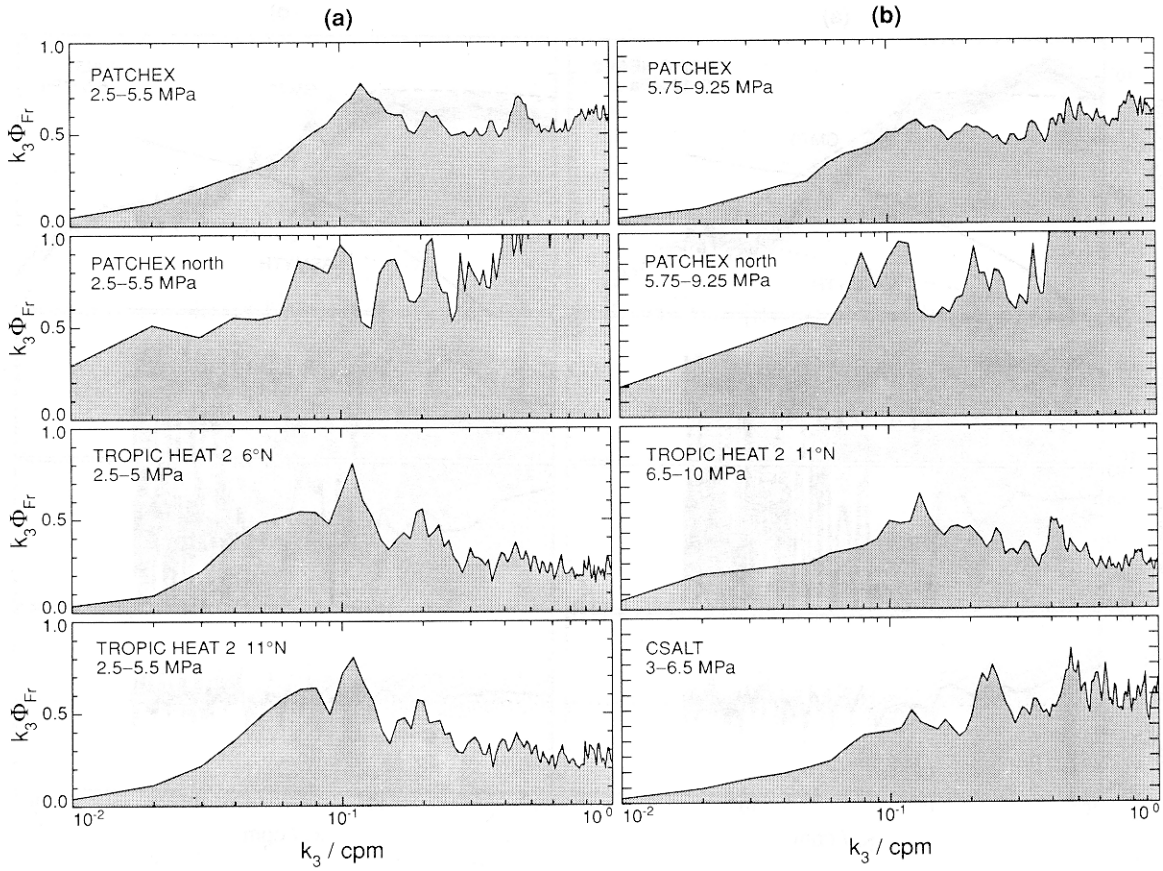

Figure 8: Variance-preserving plots of the internal wave spectra. The deep PATCHEX spectrum is closest to GM76 and has uniform contributions to the variance in the rolloff between 0.1 and 1 cpm. Both PATCHEX north spectra rise rapidly near 0.4 cpm, where turbulence becomes the dominant signal. The TH2 spectra have broad maxima centered at 0.08 cpm; hence a weak spectral gap separates internal waves from turbulence. Several spectra have local maxima near 0.1 cpm, indicating concentrations of variance at the beginning of the rolloff.

integrating (7), we would expect the kinetic energy at 6° to be $f_{34°}/f_{6°} = 5.4$ times higher than PATCHEX. Instead, we find the kinetic energy at 6°N to be 0.83 times PATCHEX. With only three profiles, this could be a statistical anomaly, but finding the same spectrum and level at 11°N suggests that this condition prevailed over a large area, at least in the spring of 1987. Moreover, we would have expected the level at 11°N to be half of that at 6°N. To the contrary, we find little difference. We conclude, therefore, that (7) may not be an accurate representation of the latitudinal structure of the internal wave field.

Analogous to the Richardson function used by Munk (1981), we quantify the shear variance with the Froude function

$$Fr(k_3) \equiv \int_{k_L}^{k_3} \Phi_{Fr}(\xi)\, d\xi \tag{18}$$

Table 3: Variances and evaluations of proposed universal constants. $\frac{KE}{KE_{GM}}$ is the ratio of kinetic energy in the observed spectrum to that in GM76 digitized and integrated numerically over the same wavenumbers. Spectra with 3.5 MPa data windows were integrated from bounds of 0.004 cpm, and the others from 0.01 cpm. Values of k_{k-1} are taken from Table 4.

Cruise	p	$\frac{KE}{KE_{GM}}$	$\left(\frac{KE}{KE_{GM}}\right) \times k_{Fr=1}$	$\left(\frac{KE}{KE_{GM}}\right) \times k_{k-1}$
	MPa		cpm	cpm
PATCHEX	2.50–5.50	0.86	0.15	0.10
PATCHEX	5.75–9.25	0.64	0.13	0.06–0.07
PATCHEX north	2.50–5.50	3.86	0.23	0.15–0.42
PATCHEX north	5.75–9.25	4.23	0.30	0.17–0.55
TROPIC HEAT 2 6°N	2.50–5.0	0.71	0.13	0.06–0.09
TROPIC HEAT 2 11°N	2.50–5.50	0.81	0.13	0.06–0.11
TROPIC HEAT 2 11°N	6.50–10.0	1.38	0.35	0.12–0.19
CSALT	3.00–6.50	0.71	0.18	0.06–0.09

where the lower limit, k_L, makes little difference because the principal contributions come from about a decade of wavenumbers in the middle or high end of the internal wave band, resulting in well-resolved shear variances and many degrees of freedom. Overlaying the Froude functions (Fig. 9) reveals PATCHEX north standing well above the others. The others vary, but much less than the differences between any of them and PATCHEX north. For example, at 0.01 cpm the deep spectrum from 11°N is largest of those in the 'pack,' but at 2 cpm it is less than PATCHEX. Froude functions are also plotted on Figures 4 to 7, and in Table 4 they are evaluated at several significant wavenumbers.

We choose k_{IW} as the wavenumber where an increase in slope marks the start of the dissipation range. PATCHEX and CSALT spectra have only minor inflections marking k_{IW}, but, owing to the more rapid internal wave rolloff, the TROPIC HEAT 2 spectra exhibit well-defined changes. For all cases, $k_{IW} < k_B$, often by about a factor of 2. For PATCHEX north, k_{IW} occurs at 0.3 and 0.4 cpm, where the k_3^{-1} rolloff ends and the slope changes to $k_3^{+1/3}$. We also see that k_B occurs at 0.7 and 0.6 cpm, the beginning of the inertial subrange. We have yet to investigate overturning scales thoroughly in the scalar records, but, as the inertial subrange implies isotropic turbulence, this narrow difference should be the transition from overturns affected by stratification to those not affected. If so, 0.3–0.7 cpm is much too narrow to be considered a buoyancy subrange.

Evaluating the Froude function at k_{IW}, the shear variance that can be assigned to internal waves has a relatively small range, corresponding to $Fr(k_{IW}) = 1.5$–2.5. Thus, in all cases the dissipation range begins well before $Fr = 4$, the necessary condition for shear instability. This does not imply that individual turbulent events do not have $Fr = 4$, only that it is not met on average throughout the profile. When we use the airfoil spectra to extend the Froude function through the dissipation range, we find that some spectra do not reach $Fr = 4$ even by the end of the dissipation range.

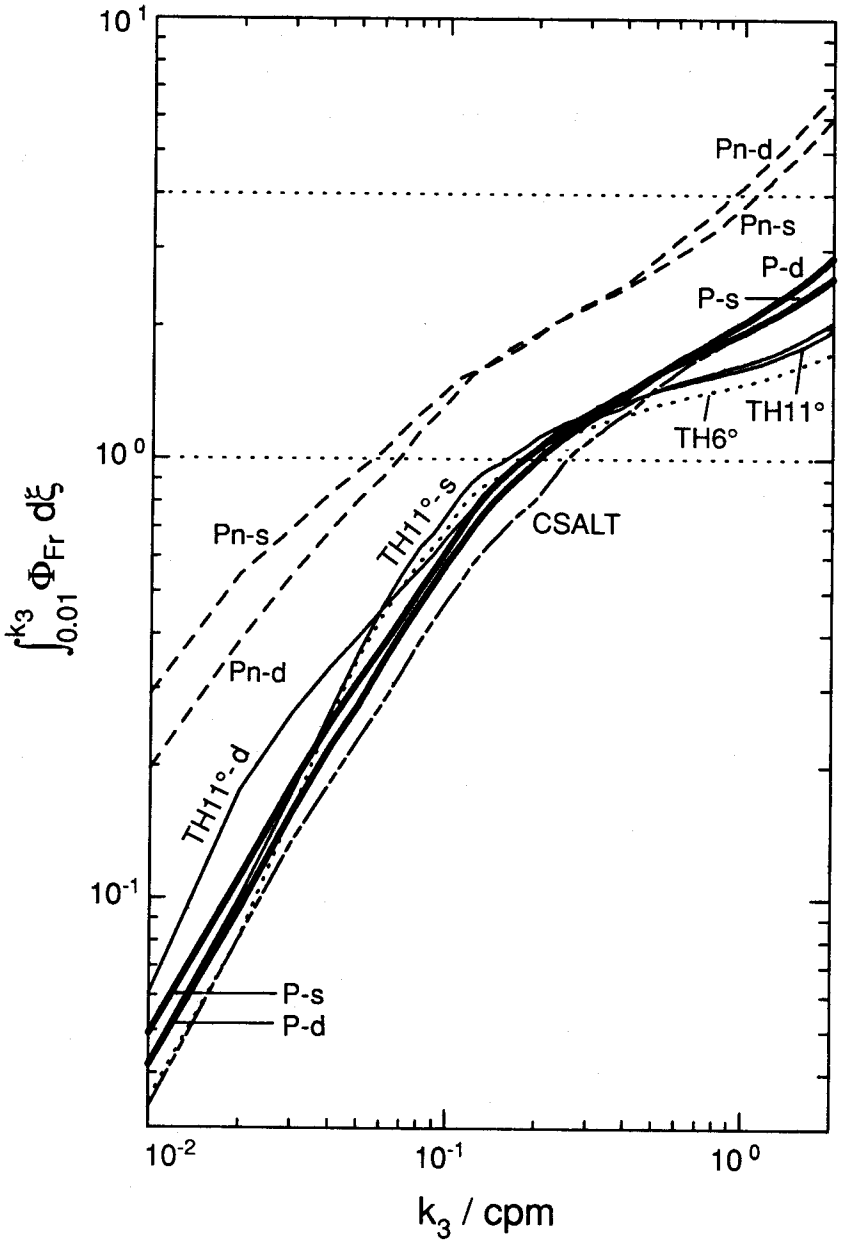

Figure 9: Comparison of all Froude functions shows two classes: PATCHEX north and the others.

The beginning of the rolloff, which we estimate visually as $k_{k^{-1}}$, is not sharply defined for most spectra, but occurs over about an octave of wavenumbers. Considering all records, the limits are 0.04 cpm $\leq k_{k^{-1}} \leq$ 0.14 cpm. Munk (1981) and Gargett et al. (1981) argue that the rolloff begins where the Froude function equals 1, i.e., $k_{Fr=1} = k_{k^{-1}}$. However, from Figures 4–7 and Table 4 we see that, except for PATCHEX north, $k_{Fr=1} = (1.5\text{–}3) \times k_{k^{-1}}$. As noted by Sherman and Pinkel (1991), this is also obtained by

integrating GM76, and it agrees with their observations for 1.5–1.8 MPa during PATCHEX. Again, PATCHEX north is the exception, having $k_{k^{-1}} = k_{\mathrm{Fr}=1}$. Why does the rolloff occur well before $k_{\mathrm{Fr}=1}$ for the other spectra? Does the mechanism of instability differ? For example, the analysis of instability in the atmosphere shows that convective overturning should precede shear instability. Aspect ratios of oceanic internal waves generally preclude convective overturning, but were conditions unusual for PATCHEX north?

Table 4: Significant wavenumbers and, in the last two columns, evaluations of the Froude function at the low and high wavenumber ends of the rolloff. Because the location of the rolloff, $k_{k^{-1}}$, is often indistinct, the estimates are made visually on intersection of the 95% confidence limits with the rolloff or its extension to lower wavenumber. Lower bound for the Froude function, $Fr(k_3)$, is 0.01 cpm.

Cruise	p MPa	$k_{k^{-1}}$ cpm	$k_{\mathrm{Fr}=1}$ cpm	k_{IW} cpm	k_{B} cpm	$Fr(k_{k^{-1}})$	$Fr(k_{\mathrm{IW}})$
PATCHEX	2.50–5.50	0.12	0.18	1.0	2.3	0.75	1.9
PATCHEX	5.75–9.25	0.09–0.11	0.20	1.0	2.0	0.52–0.64	2.0
PATCHEX north	2.50–5.50	0.04–0.11	0.06	0.3	0.7	0.83–1.53	2.2
PATCHEX north	5.75–9.25	0.04–0.13	0.07	0.4	0.6	0.69–1.60	2.5
TROPIC HEAT 2 6°N	2.50–5.00	0.08–0.13	0.19	0.9	2.7	0.58–0.86	1.5
TROPIC HEAT 2 11°N	2.50–5.50	0.08–0.13	0.16	0.8	1.8	0.63–0.93	1.6
TROPIC HEAT 2 11°N	6.50–10.0	0.09–0.14	0.25	0.8	2.6	0.61–0.87	1.6
CSALT	3.0–6.5	0.08–0.12	0.25	1.2	2.0	0.38–0.57	2.1

Because we cannot obtain the total kinetic energy from these profiles, we test (3) as

$$\frac{KE}{KE_{\mathrm{GM}}} \times k_{k^{-1}} = \text{constant} \tag{19}$$

Closely related is

$$\frac{KE}{KE_{\mathrm{GM}}} \times k_{\mathrm{Fr}=1} = \text{constant} \tag{20}$$

found by Duda and Cox (1989) to be a good representation of their profiles. In both cases, the measure of the cutoff, $k_{k^{-1}}$ or $k_{\mathrm{Fr}=1}$, varies inversely with the energy level. In neither case do (19) or (20) accurately describe our observations (Table 3). Instead, there appear to be several groups having approximately the same products. One group, containing PATCHEX, shallow TROPIC HEAT 2, and CSALT, has $(KE/KE_{\mathrm{GM}}) \times k_{\mathrm{Fr}=1} =$ 0.13–0.18 and $(KE/KE_{\mathrm{GM}}) \times k_{k^{-1}} =$ 0.06–0.11, compared with 0.23–0.30 and 0.15–0.55 for the PATCHEX north spectra, which constitute a second group. The deep spectrum from 11°N is a group by itself, with (19) close to PATCHEX north and (20) intermediate between the first two groups. In any event, neither $k_{\mathrm{Fr}=1}$ nor $k_{k^{-1}}$ decreases sufficiently to compensate the increase in kinetic energy for PATCHEX north relative to PATCHEX. Therefore, (19) and (20) fail to describe even our mid-latitude data.

VERTICAL SYMMETRY, COHERENCE, AND PHASE

Although GM76 assumes vertical symmetry, observations often reveal asymmetry. Most kinetic energy in the internal wave field resides at near-inertial frequencies and is polarized, with significant coherence between u and v. In the northern hemisphere, near-inertial motions with downward group velocity have clockwise rotation (CW, with $\phi = +90°$) and those with upward group velocity have anticlockwise rotation (ACW, with $\phi = -90°$). Rotary decomposition of velocity profiles often reveals $\Phi_{CW}/\Phi_{ACW} > 1$, corresponding to an excess of downward propagating energy (Leaman and Sanford, 1975).

At low wavenumbers, the shallow PATCHEX record has small, but significant, coh^2, $\phi \approx +90°$, and $\Phi_{CW}/\Phi_{ACW} > 1$ for $k = 0.01$–0.03 cpm (Fig. 4). (Because confidence limits for ϕ depend inversely on coh^2, ϕ is unreliable when coh^2 is insignificant.) At 0.01 cpm, the flux asymmetry is large, upward exceeding downward by nearly 2:1. The excess decreases with increasing wavenumber, and does not differ significantly from 1 for 0.04–0.07 cpm. Over nearly the same interval, coh^2 also decreases and is not significantly different from 0. Coherence-squared is again significant between 0.08–0.13 cpm and 0.16–0.2 cpm. In the first instance, $\phi \approx +60°$ (the confidence limits include $+90°$), and $\Phi_{CW}/\Phi_{ACW} > 1$, all consistent with downward propagation. In the second instance, $\phi \approx -90°$ and $\Phi_{CW}/\Phi_{ACW} < 1$, indicating upward propagation. Furthermore, replotting the spectra with a linear wavenumber axis reveals similar patterns throughout 0.1–1 cpm (Fig. 10). In these cases, however, the significance is much less.

At low wavenumbers, the deep PATCHEX record does not have significant coh^2, and Φ_{CW}/Φ_{ACW} is not significantly different from 1 (Fig. 4). The vertical symmetry of this record may be a consequence of its distance from surface forcing. Lack of coherence at low wavenumbers, however, does not appear to affect intermediate scales. Coherence-squared is significant for 0.05–1.2 cpm and 0.18–2.0 cpm, with the same pattern of phase and flux asymmetry as found in the shallow spectrum; i.e., the first coherent band has $\phi \approx +90°$ and $\Phi_{CW}/\Phi_{ACW} > 1$, the second has $\phi \approx -90°$ and $\Phi_{CW}/\Phi_{ACW} < 1$. Furthermore, using a linear wavenumber axis shows additional coherent patterns throughout the rolloff (Fig. 10).

We are not aware of previous reports of near-inertial signatures at high wavenumbers. To the contrary, after decomposing a time series of velocity profiles into mean, near-inertial, and high-frequency internal waves, Sanford (1991) finds that "At all wavelengths shorter than about 100 m, the higher-frequency waves are more energetic." Occurrence of the first coherent band at the beginning of the rolloff is a signature one would expect if the rolloff results from strong Doppler shifting creating critical layers for waves of this scale. The small magnitudes of coh^2 demonstrate that somewhat less than 10% of the variance at the rolloff scale is involved, which is plausible. Bands of coherent u and v structures throughout the rolloff are also consistent with wave/wave interactions, moving energy to higher wavenumbers until the waves break down into turbulence at $k_3 > 1$ cpm. Existence of coherent structures is also inconsistent with the rolloff being a buoyant subrange of three-dimensional turbulence.

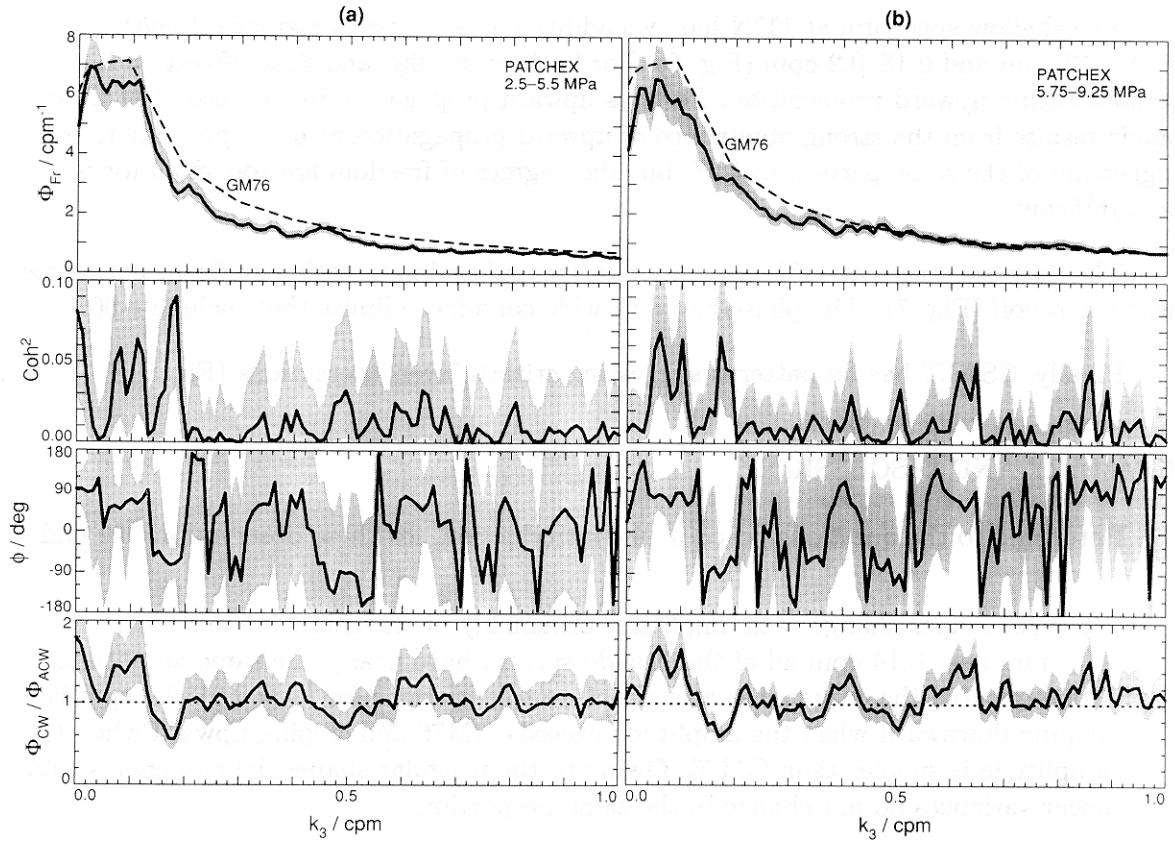

Figure 10: The PATCHEX spectra on a linear wavenumber axis. Although not as well defined as the two patterns at the beginning of the rolloff, the region from 0.1–1 cpm has numerous sections with significant coh^2, $\phi \approx \pm 90°$, and matching Φ_{CW}/Φ_{ACW} greater than or less than 1.

Similar coherent patterns occur in some of the other spectra, but, owing to fewer degrees of freedom, their significance is much less. At 0.01 cpm, the PATCHEX north spectra have $coh^2 = 0.1$–0.2, $\phi \approx +90°$, and $\Phi_{CW}/\Phi_{ACW} \geq 2$ (Fig. 5). Thus, even for the deeper record, energy at low wavenumbers is strongly dominated by downward propagating waves, and these signatures drop off with increasing wavenumber. For the shallow record, only one wavenumber near the rolloff has significant coh^2, but for the deep record the band is wider, 0.07–0.1 cpm, and coincides with the significant local spectral maximum which is very prominent in the variance-preserving plot (Fig. 8).

The shallow TROPIC HEAT 2 spectra are quite different, being dominated by upward-propagating energy: $coh^2 \approx 0.3$, $\phi \approx -90°$, and $\Phi_{CW}/\Phi_{ACW} \approx 0.3$ (Figs. 6 and 7). Curiously, coh^2 is equally large for the deep spectrum at 11°N , but $\phi \approx +90°$ and $\Phi_{CW}/\Phi_{ACW} \approx 3$. Thus, at low wavenumbers, the shallow records are strongly dominated by upward-propagating energy and the deep record is strongly dominated by downward-propagating energy, a situation we cannot explain.

The shallow spectrum at 11°N has two additional bands with significant coh^2: 0.09–0.13 cpm and 0.18–0.2 cpm (Fig. 6). For both, $\phi \approx -90°$ and $\Phi_{\rm CW}/\Phi_{\rm ACW} < 1$, demonstrating upward propagation. Perhaps upward propagation in the second of these bands results from the strong dominance of upward propagation at 0.01 cpm. There is a suggestion of the same pattern at 6°N, but the degrees of freedom are too small for it to be significant.

The deep spectrum at 11°N has only one spectral estimate with significant coherence near the rolloff (Fig. 7). The phase has very wide confidence limits that include −90°.

Finally, CSALT has no patterns suggesting critical layer interactions (Fig. 7).

SUMMARY AND DISCUSSION

Returning to the questions posed in the introduction, for these observations we find

- Spectral shapes change with amplitude principally at wavenumbers less than 0.1 cpm; near 0.14 cpm all of the Froude spectra have nearly the same amplitude. Consequently, the only systematic structure to variations for $k_3 = 0.01$–0.1 cpm is sloping downward when the amplitude exceeds GM76 and sloping upward when the amplitude is smaller than GM76. Owing to the irregular shapes, kinetic energy and shear variances do not change in the same proportion.

- Spectra from low latitudes in the central Pacific differ markedly from those at mid-latitude, but the differences are not those predicted by Munk's (1981) addition of latitude dependence to GM76. Munk predicts kinetic energies 3 and 5 times GM76 at 11°N and 6°N, respectively; whereas we observe 0.8 and 1.4 times GM76 in the shallow and deep spectra at 11°N, and 0.7 times GM76 in the shallow spectrum at 6°N. Both shallow spectra have band-limited shear variances concentrated near 0.08 cpm and roll off as $k_3^{-1.4}$, rather than as k_3^{-1} at mid-latitude. Although not as peaked as the shallow spectra, the deep spectrum at 11°N rolls off as steeply and also has a spectral gap separating internal waves and turbulence.

- The CSALT spectra are similar to PATCHEX and to GM76, the principal difference being somewhat lower levels near 0.01 cpm. In view of the different appearance of the CSALT velocity profiles, the similarity of the spectra to PATCHEX and to GM76 is unexpected. It is not clear, however, what spectral shape is typical at that latitude. The CSALT spectra, taken at 12°N, differ markedly from those observed at 11.5°N during TROPIC HEAT 2. More spectra at low latitudes are needed to define the norm, assuming one exists.

- In most of the spectra, bands of near-inertial energy (as indicated by significant coherence-squared between u and v with phases of ±90°) span the rolloff, k_{k-1}, and recur irregularly throughout the rolloff region, usually 0.1–1 cpm. These signatures are unexpected, as high-frequency waves generally dominate wavenumbers greater than 0.01 cpm (Sanford, 1991), and we interpret them as evidence of critical layer

interactions causing the rolloff. Preliminary examination of overturning scales in these profiles shows vertical scales consistent with k_B, i.e., tens of centimeters or less except for PATCHEX north which has overturns of about 1 m. Thus, in both cases, the rolloff cannot contain the three-dimensional turbulence needed for a buoyancy subrange.

- The PATCHEX north spectrum rolls off at a lower wavenumber than does the PATCHEX spectrum, as expected from the larger velocity and shear variances of PATCHEX north. The decrease in k_{k-1}, however, is only about half the decrease predicted by Munk's (1981) $E \times k_{k-1} =$ constant. For the other records, k_{k-1} shows little systematic shift with changes in kinetic energy but all of them roll off where $Fr = 0.5$–0.8.

- When evaluated with $\langle\varepsilon\rangle$, Nasmyth's spectrum adequately approximates the observed spectra in the dissipation range, particularly for the PATCHEX north records which are strongly turbulent. Our spectra, however, roll off more gradually beyond the viscous cutoff, and we do not know whether this results from the averaging procedure or is more fundamental.

Considering the range of spectral amplitudes, the variety of spectral shapes for 0.01–0.1 cpm is not surprising. Energy enters at low wavenumbers, and the spectrum is likely to contain signatures of the generation mechanisms, much like energy-containing scales of turbulence. (This is especially true for these data, which were collected at relatively shallow depths and may have sampled forced rather than freely propagating waves.) The observed departures from white shear spectra, i.e., from k_3^0, imply some degree of coherent structure in the low-wavenumber shear field. This is a general consequence of a white spectrum and a unit impulse autocorrelation function being a Fourier transform pair, and is the basis for the cumulative periodogram test for correlatedness (Jenkins and Watts, 1969). As generation mechanisms are identified, it may be possible to infer mechanisms from spectral signatures and to relate changes in kinetic energy to changes in shear. At present, however, we cannot identify the mechanisms. Nor can we accurately predict variations in shear from those in kinetic energy.

During eight days of sampling, internal waves did not change appreciably during PATCHEX. The other observations were collected much more rapidly and thus represent only snapshots. However, the similarity of the shallow spectra from 6°N and 11°N makes it plausible to assume that these also represent a steady state. Furthermore, the long time scale of the thermohaline staircase east of Barbados is strong evidence that CSALT also sampled a steady state.

In spite of significant differences in low-wavenumber shear and in the steepness of their rolloffs, PATCHEX and TROPIC HEAT 2 have nearly the same average dissipation rates, as does CSALT. These rates are minimal, slightly above 10^{-10} W kg^{-1}. Minimal dissipation rates reflect the tendency of all thermodynamic systems to evolve to states of minimum entropy production consistent with the constraints imposed upon them (De Groot and Mazur, 1962). By contrast, $\langle\varepsilon\rangle$ is not minimal for PATCHEX north.

We conclude that the most likely interpretation of the spectra and their dissipation rates is

1. PATCHEX and TROPIC HEAT 2 sampled steady states or nearly steady states of freely propagating waves close to equilibrium; i.e., the observations typify long-term averages at those sites, $\langle\varepsilon\rangle$ represents the average energy flux through the shear spectra, and the spectral shapes are adjusted to maintain that energy flux.
2. The contrast in spectral shapes between PATCHEX and TROPIC HEAT 2 results from differences in large-scale forcing of the internal wave field and in latitudinal changes in the rate at which wave/wave interactions transfer energy.
3. Either PATCHEX north was in steady state with active forcing or it was decaying from previous forcing.

In view of the limited sampling, we obviously cannot prove these statements; we regard them as hypotheses to be tested by further observations and perhaps by numerical calculations. In Figure 9, we have already noted how the Froude function for PATCHEX north stands above the others. Plotting ratios of the observed Froude functions to the Froude function for GM76 shows how these functions change with wavenumber (Fig. 11). Except for PATCHEX north, the Froude ratios converge to about 0.8, regardless of whether they start above or below 1. All of these records have low dissipation rates, as shown by the variance-preserving dissipation plots in the right-hand panels. The ratios for PATCHEX north drop with increasing wavenumber, but terminate at k_{IW}, the end of the internal wave region, before reaching 0.8. They correspond to the only high dissipation spectra. We conclude that $Fr(k_{\mathrm{IW}})$ is likely the major factor establishing $\langle\varepsilon\rangle$.

Most sampling during TROPIC HEAT 2 was concentrated on the equator, but we also profiled at 1°N and 2°N. At low wavenumbers, these profiles have Froude ratios that fill in the space in Figure 11 between PATCHEX north and the deep record at 11°N. Unlike PATCHEX north, however, the Froude ratios for the 2°N–0°N spectra drop steeply with increasing wavenumber and terminate near 0.8. They also have minimal dissipation rates and overlay the low values on the variance-preserving spectra. Owing to the strong mean shears within 2° of the equator, wave/wave interactions are likely to be more complicated than for the records we have presented. Nevertheless, the shapes of their spectra are consistent with the hypothesis that $\langle\varepsilon\rangle$ is controlled by $Fr(k_{\mathrm{IW}})$.

The rapid rolloff in the low-latitude spectra is consistent with reduced wave/wave flux feeding energy to small scales. But, if that flux is linearly proportional to f, why isn't the rolloff steeper at 6°N than at 11°N. And, why are the dissipation rates at these stations nearly the same as at PATCHEX? Because velocity and shear variances for $k_3 \leq k_{k-1}$ are comparable to PATCHEX, we expect $\langle\varepsilon\rangle$ at 11°N to be 1/3 of PATCHEX and $\langle\varepsilon\rangle$ at 6°N to be 1/5 of PATCHEX.

The location of the rolloff, k_{k-1}, shows the same two groups of profiles that we obtain from the Froude functions, namely PATCHEX north, with $Fr(k_{k-1}) \approx 1$, and the others,

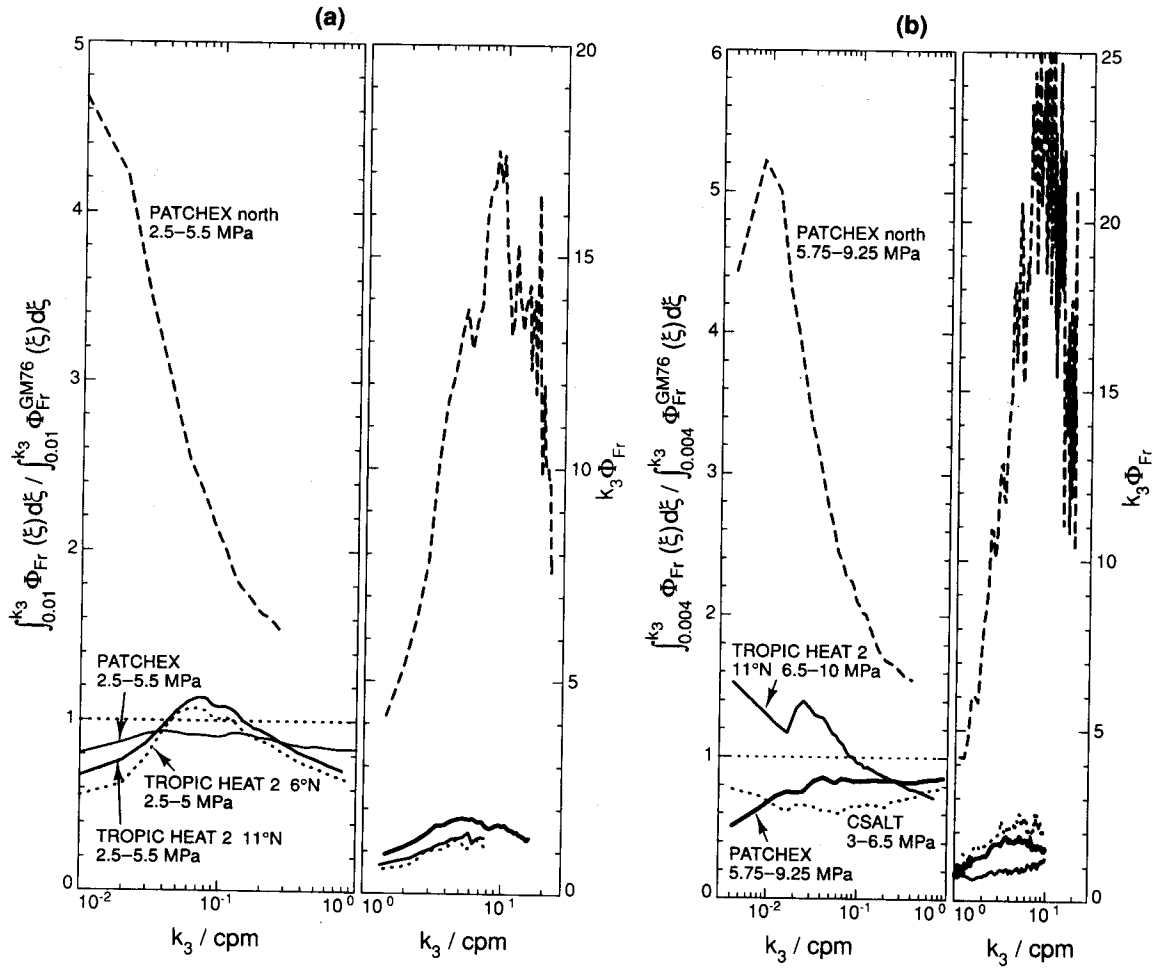

Figure 11: Ratios of observed Froude functions to the Froude function and variance-preserving dissipation spectra for shallow spectra (left) and for the deep spectra plus CSALT (right). Froude plots are cut off at k_{IW}. In spite of larger differences in amplitude and shape among the spectra, only PATCHEX north stands out.

with $Fr(k_{k-1}) \approx 0.5$. Although we do not consider the rolloff a buoyancy subrange, we applied the buoyancy scaling used by Gargett et al. (1981) to PATCHEX and PATCHEX north, which have similar values of f. The results are dramatic (Fig. 12), achieving a better collapse than obtained by Gargett et al. In addition, the collapse extends across the internal wave range and is not limited to the rolloff. If this collapse is not fortuitous, the scaling must be an internal wave scaling rather than a buoyancy scaling. As in the models of wave/wave interactions by McComas and Müller (1981) and Henyey et al. (1986), for a wave field in equilibrium $\langle\epsilon\rangle$ is also the rate at which energy flows through the spectrum. In which case, the striking collapse of PATCHEX and PATCHEX north indicates that the shape of the PATCHEX north spectrum is close to that required to maintain a uniform energy flux.

Occurrence of the rolloff at 0.1 cpm, instead of near 0.013 cpm as predicted by Holloway (1980), indicates that $c_h \approx u_{RMS}$ is not the criterion for Doppler shifts leading to

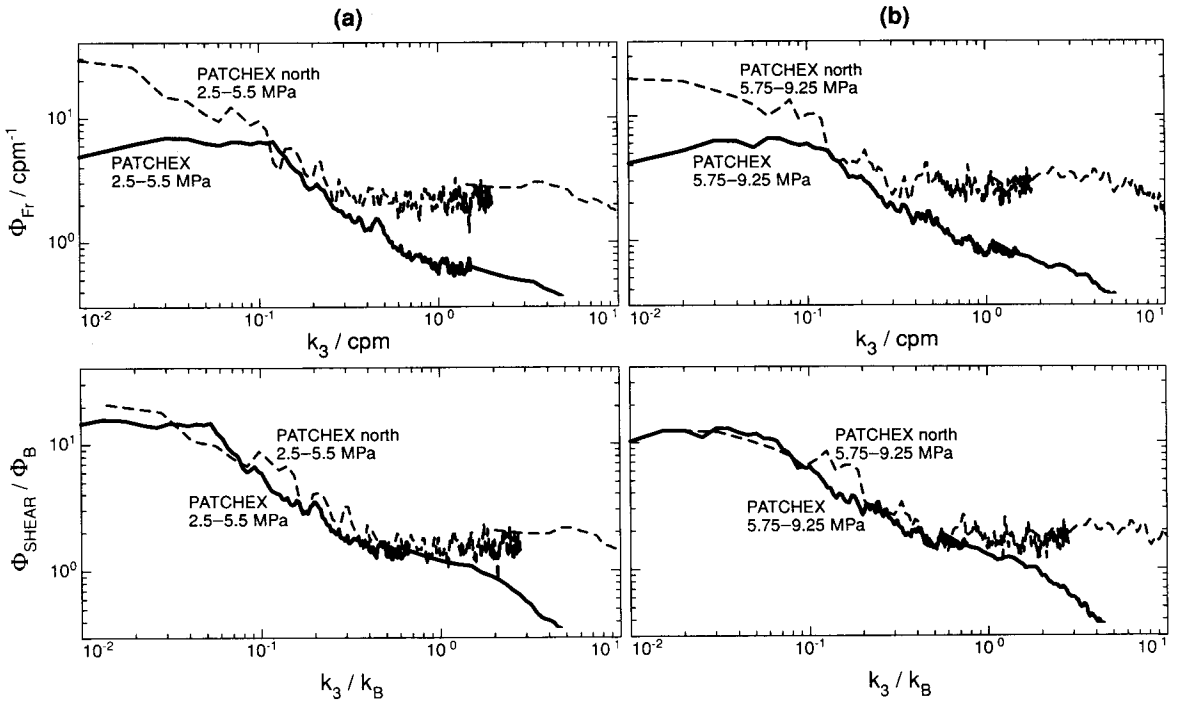

Figure 12: Froude and buoyancy scalings applied to the shallow (left) and deep (right) spectra from PATCHEX and PATCHEX north. The buoyancy scaling gives a much better collapse throughout the internal wave range, $k_3/k_B < 1$ in our interpretation, but not in the turbulent range, $k_3/k_B > 1$.

critical layers. We suggest two reasons for the apparent discrepancy in the scale of the rolloff: 1) The probability distribution for velocity differences produced by large-scale waves is skewed. Consequently, even though $ch \approx u_{\mathrm{RMS}}$ at 0.013 cpm, half or more of the distribution at that scale has smaller velocity differences. 2) Critical layers also require alignment in direction between the 'test' wave and the field of the large-scale waves. For a horizontally isotropic wave field, this further reduces the likelihood of a critical layer when $ch \approx u_{\mathrm{RMS}}$.

When u and v are normally distributed, $u^2 + v^2$ has a chi-square distribution (when suitably normalized), which is skewed. Consequently, the most probable velocity difference experienced by a wave is less than u_{RMS}. In Figure 13, we show probability density functions of $\log_{10}[(\Delta u)^2 + (\Delta v)^2]$ for a range of Δz. For PATCHEX, when $\Delta z = 50$ m, corresponding to $c_h \approx u_{\mathrm{RMS}}$, half of the velocity differences are less than c_h^2, and the probability of matching amplitude and direction must be relatively low. For $\Delta z = 10$ m, however, only a few percent of the velocity differences are less than c_h^2, and the probability of matching amplitude and direction must be much larger. The probability densities for PATCHEX north are not as well defined, but show few velocity differences less than c_h^2 for $\Delta z = 50$–25 m, consistent with the rolloff beginning at lower wavenumbers.

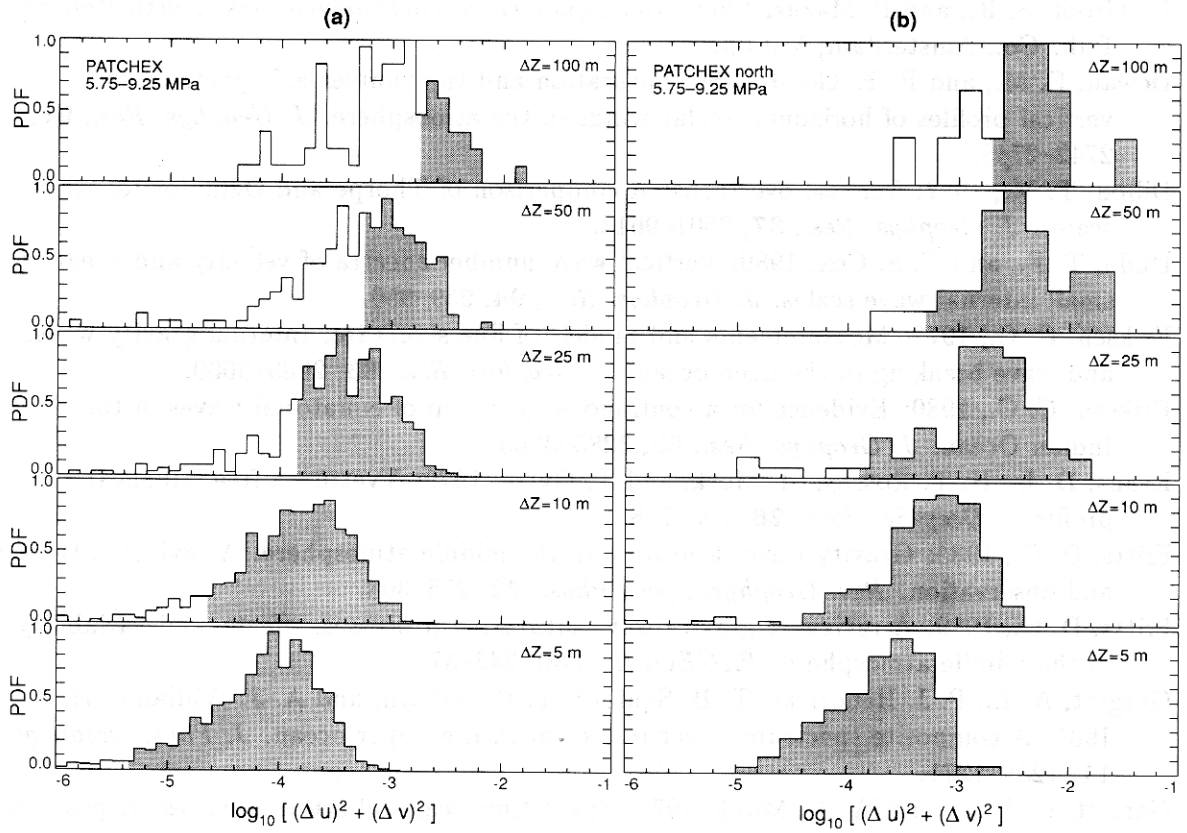

Figure 13: Probability density functions of $(\Delta V)^2$ for different vertical lengths, Δz. Shading shows where $\Delta V \geq c_h$, the horizontal phase speed of internal waves having the same vertical scale. The histograms are fully shaded only when $\Delta z \leq 10$ m.

Much of this discussion is speculation in an attempt to formulate the hypotheses needed to move from internal wave kinematics to dynamics. These records demonstrate that, until we better understand dynamics, we need to continue fully resolving the vertical shear spectrum. Further observations are needed to determine the full range of shapes and amplitudes for shear spectra, but, even more, to reveal how these characteristics evolve during strong forcing.

Acknowledgments. Collection of the MSP data was funded by the Office of Naval Research and the National Science Foundation. The Office of Naval Research funded this analysis through the *Mixing to Mesoscale* University Research Initiative at the University of Washington (Contract N00014–86–K–0690). Don Percival and Harvey Seim provided useful discussions and comments. Contribution 1891 of the School of Oceanography.

REFERENCES

Bendat, J. S., and A. G. Piersol, 1971: *Random Data: Analysis and Measurement Procedures.* Wiley-Interscience, New York, 407 pp.

De Groot, S. R., and P. Mazur, 1962. *Non-Equilibrium Thermodynamics*. North-Holland Pub. Co., Amsterdam, 510 pp.

Dewan, E. M., and R. E. Good, 1986: Saturation and the "universal" spectrum for vertical profiles of horizontal scalar winds in the atmosphere. *J. Geophys. Res.*, **91**, 2742–2748.

Dillon, T. M., 1982: Vertical overturns: A comparison of Thorpe and Ozmidov length scales. *J. Geophys. Res.*, **87**, 9601–9613.

Duda, T. F., and C. S. Cox, 1989: Vertical wave number spectra of velocity and shear at small internal wave scales. *J. Geophys. Res.*, **94**, 939–950.

Eriksen, C. C., 1978: Measurements and models of fine structure: Internal gravity waves, and wave breaking in the deep ocean. *J. Geophys. Res.*, **83**, 2989–3009.

Eriksen, C. C., 1980: Evidence for a continuous spectrum of equatorial waves in the Indian Ocean. *J. Geophys. Res.*, **85**, 3285–3303.

Evans, D. L., H. T. Rossby, M. Mork, and T. Gytre, 1979: Yvette—a free-fall shear profiler. *Deep-Sea Res.*, **26**, 703–718.

Fritts, D. C., 1984: Gravity wave saturation in the middle atmosphere: A review of theory and observation. *Rev. Geophys. Space Phys.*, **22**, 275–308.

Fritts, D. C., 1989: A review of gravity wave saturation processes, effects, and variability in the middle atmosphere. *PAGEOPH.*, **130**, 343–371.

Gargett, A. E., P. J. Hendricks, T. B. Sanford, T. R. Osborn, and A. J. Williams III, 1981: A composite spectrum of vertical shear in the upper ocean. *J. Phys. Oceanogr.*, **11**, 1258–1271.

Garrett, C. J. R., and W. H. Munk, 1975: Space-time scales of internal waves: A progress report. *J. Geophys. Res.*, **80**, 291–297.

Gregg, M. C., 1977a: A comparison of finestructure spectra from the main thermocline. *J. Phys. Oceanogr.*, **7**, 33–40.

Gregg, M. C., 1977b: Variations in the intensity of small-scale mixing in the main thermocline. *J. Phys. Oceanogr.*, **7**, 436–454.

Gregg, M. C., 1989: Scaling turbulent dissipation in the thermocline. *J. Geophys. Res.*, **94**, 9686–9698.

Gregg, M. C., and E. Kunze, 1991: Shear and strain in Santa Monica Basin. *J. Geophys. Res.*, in press.

Gregg, M. C. and T. B. Sanford, 1987: Shear and turbulence in thermohaline staircases. *Deep-Sea Res.*, **34**, 1689–1696.

Gregg, M. C., and T. B. Sanford, 1988: The dependence of turbulent dissipation on stratification in a diffusively stable thermocline. *J. Geophys. Res.*, **93**, 12,381–12,392.

Gregg, M. C., C. S. Cox, and P. W. Hacker, 1973: Vertical microstructure measurements in the central North Pacific. *J. Phys. Oceanogr.*, **3**, 458–469.

Gregg, M. C., H. Seim, and D. B. Percival, 1991: Statistics of shear and turbulent dissipation in profiles. *J. Geophys. Res.*, submitted.

Hayes, S. P., H. B. Milburn, and E. F. Ford, 1984: TOPS: a free-fall velocity and CTD profiler. *J. Atmos. Oceanic Technol.*, **1**, 220–236.

Henyey, F.S., J. Wright, and S. M. Flatté, 1986: Energy and action flow through the internal wave field: An eikonal approach. *J. Geophys. Res.*, **91**, 8487–8495.

Hess, W. C., D. B. Percival, and M. C. Gregg, 1991: Robust estimation of the rate of turbulent dissipation. (in preparation)

Hines, C. O., 1991a: The saturation of gravity waves in the middle atmosphere. Part I: Critique of linear-instability theory. *J. Atmos. Sci.*, in press.

Hines, C. O., 1991b: The saturation of gravity waves in the middle atmosphere. Part II: Development of Doppler-spread theory. *J. Atmos. Sci.*, in press.

Holloway, G., 1980: Oceanic internal waves are not weak waves. *J. Phys. Oceanogr.*, **10**, 906–914.

Jenkins, G. M. and D. G. Watts, 1969: *Spectral Analysis and Its Applications*. Holden-Day, San Francisco, 525 pp.

Leaman, K. D., and T. B. Sanford, 1975: Vertical energy propagation of inertial waves: A vector spectral analysis of velocity profiles. *J. Geophys. Res.*, **80**, 1975–1978.

Levine, M. D., C. A. Paulson, and J. H. Morison, 1985: Internal waves in the Arctic Ocean: Comparison with lower-latitude observations. *J. Phys. Oceanogr.*, **15**, 800–809.

Lumley, J. L., 1964: The spectrum of nearly inertial turbulence in a stably stratified fluid. *J. Atmos. Sci.*, **21**, 99–102.

McComas, C. H., and P. Müller, 1981: The dynamic balance of internal waves. *J. Phys. Oceanogr.*, **11**, 970–986.

Munk, W. H., 1981: Internal waves and small-scale processes. In *Evolution of Physical Oceanography, Scientific Surveys in Honor of Henry Stommel*, edited by B. A. Warren and C. Wunsch, 264–291, MIT Press, Cambridge, Mass.

Oakey, N. S., 1982: Determination of the rate of dissipation of turbulent energy from simultaneous temperature and velocity shear microstructure measurements. *J. Phys. Oceanogr.*, **12**, 256–271.

Percival, D., 1991: A note on confidence intervals for the magnitude squared coherence. *J. Time Ser. Anal.*, submitted.

Sanford, T. B., 1991: Spatial structure of thermocline and abyssal internal waves. This volume.

Sherman, J. T., and R. Pinkel, 1991: Estimates of the vertical wavenumber-frequency spectra of vertical shear and strain. *J. Phys. Oceanogr.*, **21**, 292–303.

Shur, G. N., 1962: Experimental studies of energy spectrum of atmospheric turbulence. *Tr. Tsent. Aerolog. Observ.*, **43**, 79–90.

Singleton, R. C., 1969: An algorithm for computing the mixed radix fast Fourier transform. *IEEE Trans. Audio and Electroacoustics*, **AU-17**, 93–103.

Smart, J. H., 1988: Comparison of modelled and observed dependence of shear on stratification in the upper ocean. *Dyn. Atmos. Oceans*, **12**, 127–142.

Smith, S. A., D. C. Fritts, and T. E. VanZandt, 1987: Evidence for a saturated spectrum of atmospheric gravity waves. *J. Atmos. Sci.*, **44**, 1404–1410.

Wunsch, C. and S. Webb, 1979: The climatology of deep ocean internal waves. *J. Phys. Oceanogr.*, **9**, 235–243.